frontiers in Earth Science

ORIGINAL RESEARCH
published: 08 May 2020
doi: 10.3389/feart.2020.00121

Southward-Directed Subduction of the Farallon–Aluk Spreading Ridge and Its Impact on Subduction Mechanics and Andean Arc Magmatism: Insights From Geochemical and Seismic Tomographic Data

Sofía B. Iannelli[1,2], Lucía Fernández Paz[1,2], Vanesa D. Litvak[1,2], Guido Gianni[1,2], Lucas M. Fennell[1,2], Javiera González[3], Friedrich Lucassen[4], Simone Kasemann[4], Verónica Oliveros[3] and Andrés Folguera[1,2]*

[1] Departamento de Ciencias Geológicas, Universidad de Buenos Aires, Buenos Aires, Argentina, [2] Instituto de Estudios Andinos 'Don Pablo Groeber', CONICET- Universidad de Buenos Aires, Buenos Aires, Argentina, [3] Departamento de Ciencias de la Tierra, Universidad de Concepción, Concepción, Chile, [4] MARUM - Center for Marine Environmental Sciences and Faculty of Geosciences, University of Bremen, Bremen, Germany

OPEN ACCESS

Edited by:
Marina Manea, National Autonomous University of Mexico, Mexico

Reviewed by:
Luca Ferrari, Geosciences Center, National Autonomous University of Mexico, Mexico
Jiashun Hu, California Institute of Technology, United States

***Correspondence:**
Sofía B. Iannelli
sofia.iannelli@hotmail.com.ar

Specialty section:
This article was submitted to Structural Geology and Tectonics, a section of the journal Frontiers in Earth Science

Received: *14 December 2019*
Accepted: *30 March 2020*
Published: *08 May 2020*

Citation:
Iannelli SB, Fernández Paz L, Litvak VD, Gianni G, Fennell LM, González J, Lucassen F, Kasemann S, Oliveros V and Folguera A (2020) Southward-Directed Subduction of the Farallon–Aluk Spreading Ridge and Its Impact on Subduction Mechanics and Andean Arc Magmatism: Insights From Geochemical and Seismic Tomographic Data. Front. Earth Sci. 8:121. doi: 10.3389/feart.2020.00121

Since the initial proposal of the past existence of a southward-directed mid-ocean ridge–subduction interaction in the Andes during Late Cretaceous–Paleogene times, several studies have been devoted to uncover the tectonomagmatic evidence of this process. The collision of a spreading ridge against a subduction margin provokes important tectonomagmatic changes, including, between them, variations in arc-related magmatic activity and in the plate-margin stress regime. However, the cryptic nature of the geological record often hampers assessing the influence and along-strike evolution of this process. In this study, we integrate new isotopic data with previous field and geochemical data on Andean arc-related magmatism, together with seismic tomography to track the main tectonic changes that affected the Andes between 35° and 42°S from Latest Cretaceous to early Miocene times. In particular, we carry out a new tomotectonic analysis combining the regional bedrock record of the Late Cretaceous–early Miocene arc with upper–lower mantle seismic tomography. This analysis allowed us to unravel the main geodynamic changes that affected the Andean active-margin when the Farallon–Aluk spreading ridge was subducting. Besides, new isotopic analyses reveal the variable nature of the mantle source that fed the Late Cretaceous–early Miocene arc. Hence, the integration of geological, geochemical, and geophysical data, together with new isotopic data studying the geochemical

composition of the main Andean arc-related magmatic units in three main periods – (1) Latest Cretaceous–early Paleocene, (2) Early Paleocene–late Eocene, and (3) Late Eocene–early Miocene – allow us to understand with an unprecedented detail the geochemical and spatiotemporal evolution of the passage of this spreading ridge along the Andean margin.

Keywords: Southern Central Andes, spreading ridge subduction, Farallon–Aluk spreading ridge, Andean magmatism, Late Cretaceous–Cenozoic period

INTRODUCTION

The subduction of oceanic spreading ridges causes a significant impact on active margins producing multiple thermal, deformational, and magmatic effects and leaving a unique geological signature on overriding plates (e.g., DeLong et al., 1979; Thorkelson, 1996). During ridge subduction, sublithospheric divergence of oceanic plates provokes the unzipping of the mid-ocean ridge leading to the formation of slab windows (e.g., Dickinson and Snyder, 1979; Groome and Thorkelson, 2009). This phenomenon produces a slab gap that allows the sub-oceanic asthenosphere to well up in a complex 3-D mantle flow (e.g., Guillaume et al., 2010). The localized mantle upwelling causes a high heat flow area, often interrupting subduction-related magmatic activity, and produces dynamic uplift of the overriding plate driving major relief and drainage reorganizations in the upper-plate surface (Guillaume et al., 2009; Ávila and Dávila, 2018). The geological signature of this process can be tracked from the forearc to the back-arc regions of active margins and its distinctive character has allowed researchers to identify this process back to Precambrian times (e.g., Santosh and Kusky, 2010). In particular, in the back-arc area, variable degrees of mantle melting in the upwelling asthenosphere generate alkaline or tholeiitic magmas with OIB signatures (e.g., Gorring et al., 1997; D'Orazio et al., 2000; Gorring and Kay, 2001). In certain cases, partial fusion of young oceanic crust in the slab window edges forms magmas of adakitic composition (e.g., Kay et al., 1993; Johnston and Thorkelson, 1997). Intraplate magmatic activity in this area is often accompanied by extensional to transtensional tectonic activity (e.g., Thorkelson, 1996; Windley and Xiao, 2018). Identifying the precise location of past slab window event is a challenging task as these effects are time transgressive and are controlled by triple-junction kinematics (Thorkelson, 1996). This is further complicated in settings where mid-ocean ridge subduction took place obliquely to the subduction zone producing a time–space migration of the slab window process along the active margin. The latter tectonic configuration has been suggested in plate kinematic reconstructions in the southeast Pacific Ocean indicating that the Farallon–Aluk mid-ocean ridge should have subducted obliquely beneath the Andes sometime during Late Cretaceous to Paleogene times (Cande and Leslie, 1986; Ramos and Kay, 1992; Aragón et al., 2011; Somoza and Ghidella, 2012; Eagles and Scott, 2014; Iannelli et al., 2018; Fennell et al., 2019).

Recent plate kinematic reconstructions suggest that the Farallon–Aluk mid-ocean ridge collided against the Andean margin at ∼30°S during the Late Cretaceous (∼80 Ma) and started migrating southwards reaching Patagonian latitudes (∼42°S) by Eocene times (Cande and Leslie, 1986; Somoza and Ghidella, 2005; Aragón et al., 2011; Somoza et al., 2012; Eagles and Scott, 2014; Müller et al., 2016; Wright et al., 2016). Along these latitudes, the emplacement of scattered magmatic sequences with contrasting geochemical signatures and the development of magmatic lulls between Late Cretaceous to Eocene times have been associated with the development of slab windows directly linked to the progressive southward sweeping of this oceanic ridge (Ramos and Kay, 1992; Muñoz et al., 2000; Aragón et al., 2011; De La Fuente, 2014; Jalowitzki et al., 2017; Gianni et al., 2018a; Iannelli et al., 2017, 2018). Contrastingly, late Eocene–Oligocene magmatism show arc-related signature with no influence from the slab window (Iannelli et al., 2017; Fernández Paz et al., 2019). Furthermore, although there is much evidence in favor of the Aluk–Farallon ridge subduction, other authors question the existence of a slab window and link this important extensional stage and the voluminous magmatism to a diminished plate coupling (Ladino et al., 2000; Muñoz et al., 2018). Moreover, several aspects associated with this complex tectonic stage in the Andean evolution remain under debate. For instance, the precise location of the triple junction during the oldest stage in the Late Cretaceous remains partially uncertain (Somoza et al., 2012; Wright et al., 2016). Thus, a regional comparison of the geochemical signature of the arc-related products, from the Late Cretaceous to the Oligocene, would allow tracking the influence of this spreading ridge over the Andean margin.

In this study, we provide new isotopic data from three arc-related magmatic units located in key segments along the Andes between 35° and 42°S and integrate it with its previous field and geochemical data to test the potential influence of the southward migration of the Farallon–Aluk ridge over Andean magmatism between the Late Cretaceous to early Miocene times. These arc-related units include Los Ángeles Unit magmatism (67 Ma) at the Southern Central Andes (35°30′S); the Eocene Huitrera Formation (44 Ma) at the North Patagonian Andes (40°S) and the Auca Pan Formation (29 Ma) located in the transitional area between Southern Central and North Patagonian Andes (39°S) (Iannelli et al., 2017, 2018). To better evaluate the regional influence of the spreading ridge on Andean magmatism, we integrate geochemical evolution of these arc-related units with available geochemical data from coeval magmatic sequences from the whole arc region between the studied latitudes (35–42°S) (e.g., Kay et al., 2006; Zamora Valcarce et al., 2006). Thus, we focus the regional integrated study on three Andean magmatic stages: (1) the Latest Cretaceous–early Paleocene (80–59 Ma), (2)

the Paleocene–Eocene (59–37 Ma), and (3) the late Eocene–early Miocene (37–20 Ma).

Also, to locate the ancient positions of potential slab windows, we use a novel approach that combines plate kinematic reconstructions with the mantle structure illuminated by global seismic tomography (Gianni et al., 2019), which is suggested to retain previous subduction configurations back to Mesozoic times (van der Meer et al., 2010, 2012). These analysis aims to test the existence of preserved slab gaps that could match the geological record of slab window position and triple junction location derived from the recent plate kinematic model of Müller et al. (2016).

Hence, by integrating seismic tomography of the uppermost lower mantle with plate kinematic reconstructions and new and existing geochemical data from Andean arc magmatism, we can track the main geodynamic and tectonic changes that affected the Andes from Latest Cretaceous to early Miocene times. Finally, a new model based on this multidisciplinary approach is presented, which supports the collision and subsequent migration of the Farallon–Aluk spreading ridge since at least the Late Cretaceous times.

REGIONAL SETTING

In the following subsections, we describe the geology of the main morphostructural units of the Southern Central Andes between 35°S and 42°S. These subsections are divided according to the main studied areas: the first in the Southern Central Andes where Late Cretaceous Los Ángeles Unit (67 Ma; 35°30'S) is emplaced, and the second one in the North Patagonian Andes where Eocene Huitrera Formation (44 Ma; 40°S) and Oligocene Auca Pan Formation (29 Ma; 39°S) crop out.

Geology of the Southern Central Andes (35–36°S)

The first studied area is located in the Southern Central Andes (35–36°S) along the Malargüe fold and thrust belt (**Figures 1**, **2**). The oldest outcrops in this Andean orogenic segment correspond to the Upper Permian–Lower Triassic Choiyoi Group (**Figure 2**; Kleiman and Japas, 2009; Sato et al., 2015), which comprise mesosilicic to silicic ignimbrites, granite intrusions, and subvolcanic domes (Llambías et al., 2003). By Late Triassic–early Cretaceous times, back-arc extension triggered the development of the Neuquén Basin, which initially started in the Late Triassic as unconnected depocenters that were filled by an alternation of non-marine to volcanic deposits (Precuyo Group). Subsequently, during the Early Jurassic back-arc extension, the depocenters were connected and filled by interbedded continental and marine deposits (Cuyo Group) (Legarreta and Uliana, 1991; Nullo et al., 2005).

The westward motion of the South American plate in the Late Cretaceous along with a shallowing of the subduction angle provoked a shift toward a compressional regime that turned the extensional retroarc Neuquén Basin into a foreland basin (Ramos and Folguera, 2005; Somoza and Zaffarana, 2008; Gianni et al., 2018a). This period was dominated by the deposition of fluvial, aeolian, and shallow lacustrine continental sequences (Neuquén Group). In the latest Cretaceous, an extensional regimen developed represented by the Malargüe Group, together with the development of a magmatic arc east of the main Andean range (**Figure 2**; Aguirre Urreta et al., 2011; Llambías and Aragón, 2011; Spagnuolo et al., 2012). Latest Cretaceous–early Paleocene volcanism is scattered along the Andean margin (**Figure 1**), including at least three units: Plan de los Yeuques Formation (34°30′S), Los Ángeles Unit (35°30′S), and the Naunauco Group (36–38°S). In the studied area, Late Cretaceous Los Ángeles Unit crop out (67 Ma; 35°30′S), characterized by basaltic to andesitic lava flows interbedded with volcanic breccias and fine- to coarse-grained sandstones, intruded by subvertical basaltic dykes (**Figures 1**, **2**). West of the studied area, the Plan de los Yeuques Formation developed between ∼80 and 63 Ma composed of andesitic lavas, volcanic breccias, and tuffs with interbedded continental deposits (Mosolf, 2013; Muñoz et al., 2018). Southwards (36–38°S), Late Cretaceous–early Paleocene arc-related magmatism (Naunauco Group; e.g., Zamora Valcarce et al., 2006; Llambías and Aragón, 2011; Mateo-Fernández Caso et al., 2011; Salvioli et al., 2017) took place in an eastern retroarc position interbedded with the synorogenic deposits of the Malargüe Group, while intrusive bodies dominate the main Andean magmatism (**Figure 1**; e.g., Franchini et al., 2003; Lucassen et al., 2004; Ramos and Folguera, 2005; Kay et al., 2006; Spagnuolo et al., 2012).

Between the Paleocene and the early Eocene, a magmatic hiatus is described in the study area (Mosolf et al., 2019), while southwards (37–38°S), volcanism remains with a calc-alkaline composition and a strong arc signature (PVNM; *Provincia Volcánica Neuquino Mendocina*) (Llambías and Rapela, 1989).

The break-up of the Farallon plate and the beginning of the Nazca plate orthogonal subduction changed drastically the tectonic conditions by late Oligocene–early Miocene times (Cande and Leslie, 1986; Somoza and Ghidella, 2005). As a consequence, an extensional regime spread along the Andean margin, developing intra-arc volcanic basins. This volcanism is included in the Abanico Formation (∼36–20 Ma), settled along the study area as a tholeiitic arc-like magmatism (**Figures 1**, **2**; Charrier et al., 1996; Muñoz et al., 2006).

During the late Miocene, a compressional regime triggered by a slab shallowing event caused the inversion of the extensional basins, the expansion of arc magmatism, and consequently the uplift of the frontal sector of the Principal Cordillera and the San Rafael Block (Folguera et al., 2009; Silvestro and Atencio, 2009; Rojas Vera et al., 2010; Turienzo, 2010; Giambiagi et al., 2012; Turienzo et al., 2012; Litvak et al., 2015). This slab shallowing event has been recently connected to the potential subduction of the ancient Payenia plume (Gianni et al., 2017). This stage finished by 4 Ma when a re-steeping of the subducting plate led to the impact of the Payenia plume with the Andean back-arc leading to the emplacement of the Payenia Volcanic

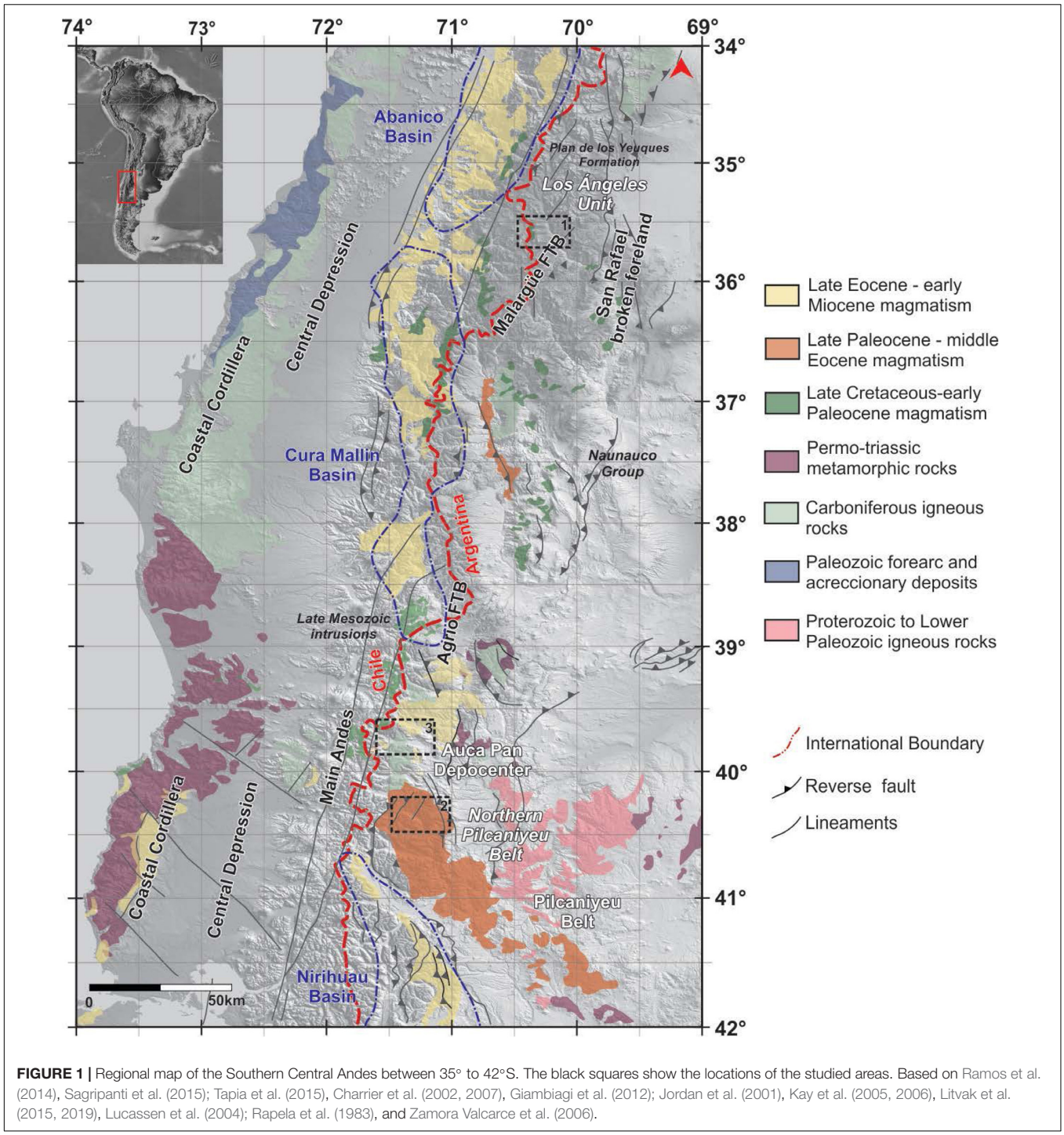

FIGURE 1 | Regional map of the Southern Central Andes between 35° to 42°S. The black squares show the locations of the studied areas. Based on Ramos et al. (2014), Sagripanti et al. (2015); Tapia et al. (2015), Charrier et al. (2002, 2007), Giambiagi et al. (2012); Jordan et al. (2001), Kay et al. (2005, 2006), Litvak et al. (2015, 2019), Lucassen et al. (2004); Rapela et al. (1983), and Zamora Valcarce et al. (2006).

Province (**Figure 2**; Llambías et al., 2010; Søager et al., 2013; Ramos et al., 2014).

Geology of North Patagonian Andes (39–41°S)

The second study area is located between 39° and 41°S and comprises the northernmost extreme of the North Patagonian Andes.

The oldest rocks of the Paleozoic basement correspond to Late Paleozoic metamorphic complex with U/Pb zircon ages between ∼420 and 380 Ma and biotite K/Ar ages between ∼375 and 310 Ma (**Figures 1**, **3**; Basei et al., 1999; Lucassen et al., 2004; Varela et al., 2005; Serra-Varela et al., 2019), whose evolution is related to the Patagonian Famatinian orogeny (Serra-Varela et al., 2019). Granites with ages between ∼350 and 270 Ma intruded the metamorphic basement (**Figure 3**;

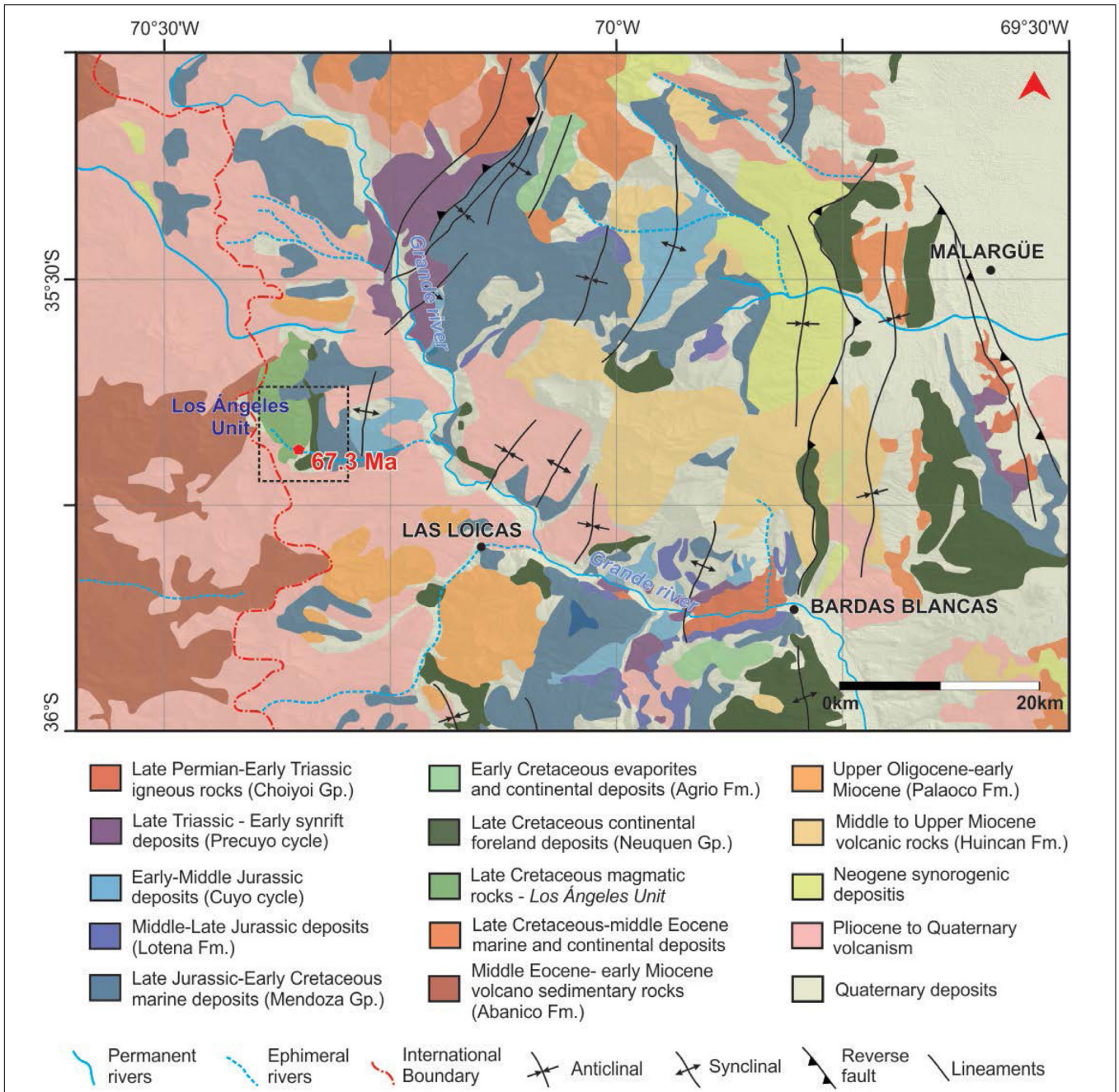

FIGURE 2 | Detailed map showing the main geological units recognized in the Southern Central Andes between 35 and 36°S. The black box shows the studied area where the Los Ángeles Unit crops out. Based on Fennell et al. (2019) and Nullo et al. (2005).

Varela et al., 1994; Basei et al., 1999; Lucassen et al., 2004) during the onset of subduction linked to the initiation of the Gondwanian orogenic cycle (Serra-Varela et al., 2019).

The Triassic to Early Jurassic period is characterized by an extensional regime that provokes the intrusion of magmatic rocks which mainly crop out in the western sector of the studied area. This magmatism is linked to the development of halfgrabens associated with the Pre-Cuyo basin filled by continental deposits (**Figure 3**; Giacosa and Heredia, 2001). Late Cretaceous magmatic rocks are emplaced to the west, mainly in the highest part of the Andes intruding the Paleozoic basement (North Patagonian Batholith; Pankhurst et al., 1999; Lucassen et al., 2004; Folguera and Ramos, 2011).

By Paleogene times (~57–43 Ma), a decrease in arc-related magmatism is registered, and intraplate-like bimodal volcanism occurred in the broken foreland area grouped in the Pilcaniyeu Magmatic Belt, also referred to as the Huitrera Formation (**Figure 1**) (~40–42°S; Rapela et al., 1988, 1984;

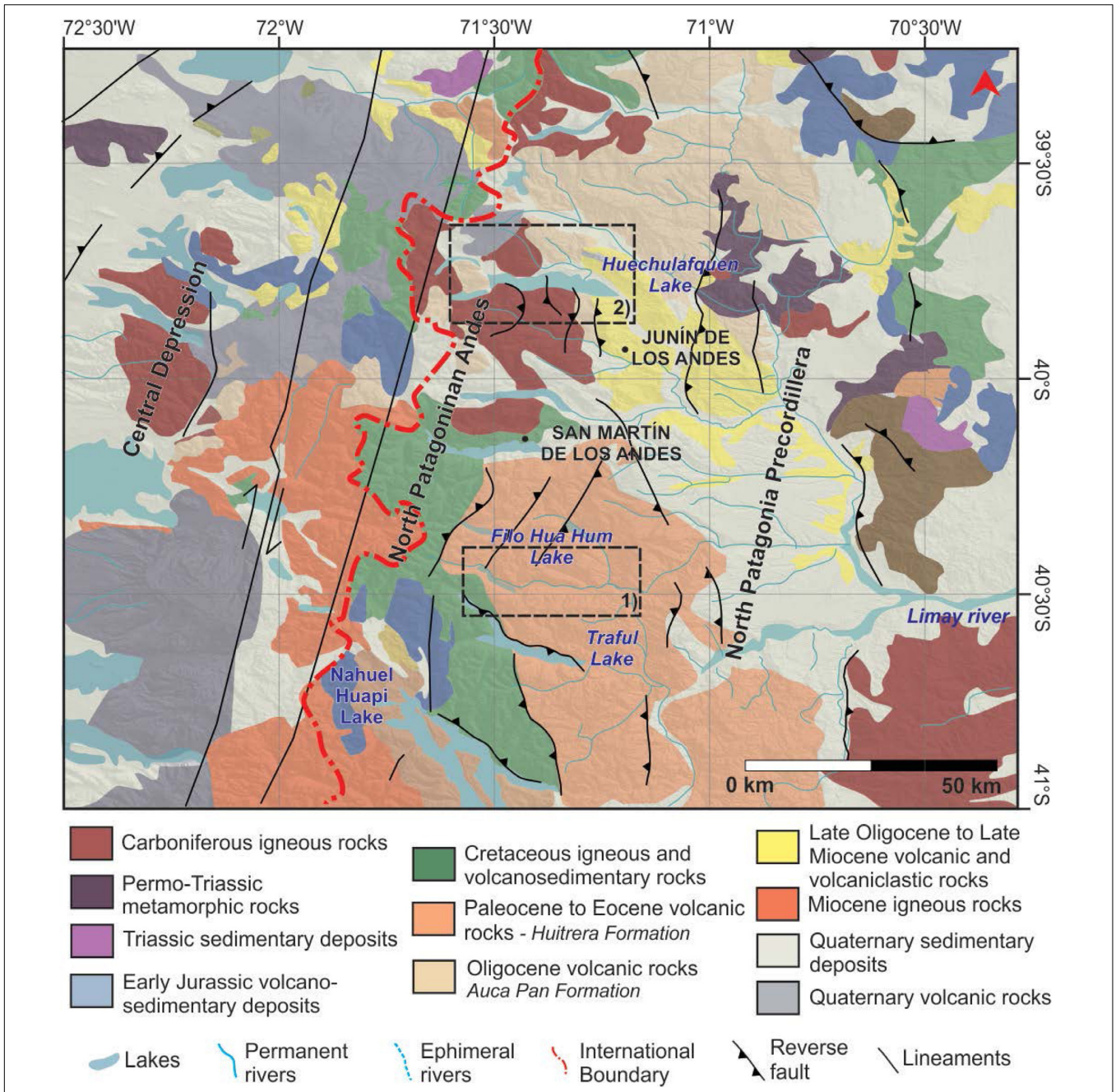

FIGURE 3 | Detailed map of the studied areas. The boxes outline the main studied areas, where (1) Paleocene to Eocene volcanic rocks crop out associated with the studied Huitrera Formation (44 Ma) and (2) Oligocene volcanic rocks appear related to the studied Auca Pan Formation (29 Ma). Modified from Ramos et al. (2014); Lucassen et al. (2004), Scasso (2012), Cazau et al. (1989), Rapela et al. (1983), and Iannelli et al. (2017).

Aragón et al., 2011; Iannelli et al., 2017). The Eocene volcanic rocks, which are one of the main focus of this paper, are located at 40°S and have been correlated with the Huitrera Formation, the northernmost and westernmost sections of the Pilcaniyeu Magmatic Belt (**Figure 3**; Iannelli et al., 2017). This magmatic stage was linked to a slab window event produced during the subduction of the Farallon–Aluk spreading ridge (Aragón et al., 2011). Afterward, the magmatic front returned to the main Andean margin by the late Eocene, represented by an arc-related volcanic belt referred to as the El Maitén Belt (González Bonorino, 1979; González Bonorino and González Bonorino, 1978; Rapela et al., 1988; Litvak et al., 2014; Fernández Paz et al., 2018, 2019). This younger volcanism (∼37–19 Ma) extended from 40° to 42°S and was mostly controlled by an extensional regime (Rapela et al., 1983; Bechis et al., 2014; Litvak et al., 2014; Fernández Paz et al., 2018, 2019). North of 40°S, the studied

Oligocene volcanic sequence is named Auca Pan Formation and is considered as the northernmost expression of this belt (Turner, 1973; Dalla Salla et al., 1981; Iannelli et al., 2017).

The latest Oligocene–early Miocene volcanic sequences were associated with the broad extensional basins induced by the rapid and orthogonal subduction of the Nazca plate and the steepening of the subducted slab (Muñoz et al., 2000; Jordan et al., 2001; Kay et al., 2006; Fennell et al., 2018). In particular, the initial infill lower section of the volcano-sedimentary Cura Mallín basin (27–20 Ma; 36–38°S) developed during this period under control of extensional structures (**Figures 1**, **3**), composed of pyroclastic deposits, lava flows, and interbedded lacustrine and delta facies (Suárez and Emparán, 1995; Jordan et al., 2001; Radic et al., 2002; Burns et al., 2006; Kay et al., 2006; Melnick et al., 2006; Folguera et al., 2010; Rojas Vera et al., 2010). To the west, the coeval Coastal Magmatic Belt developed with a predominant tholeiitic composition and variable geochemical signatures similar to the SVZ (Southern Volcanic Zone) (López-Escobar and Vergara, 1997; Muñoz et al., 2000). These volcanic rocks are interbedded with continental and marine sedimentary deposits.

During the late Miocene, a compressional regime caused the inversion of previous extensional structures with the intrusion of gabbros and leucogranites in the North Patagonian Andes, while the magmatic arc activity resurged and endures till today (Aragón et al., 2011). The intrusions emplaced mainly along dextral strike-slip system of the Liquiñe-Ofqui fault zone (LOFZ) between 19.7 and 7 Ma (Rapela et al., 1983; González Díaz and Lizuaín, 1984; Aragón et al., 2011). Furthermore, isolated within-plate magmatic bodies are also found in the Precordillera region, which have been attributed to a period of slab steepening in the late Pliocene after a restricted shallow subduction setting in the middle to late Miocene (Orts et al., 2015).

LATE CRETACEOUS TO OLIGOCENE ARC-LIKE MAGMATIC SEQUENCES FROM THE SOUTHERN CENTRAL ANDES TO THE NORTH PATAGONIAN ANDES (35–42°S)

Age and Distribution

The first and older studied sequence corresponds to the Late Cretaceous Los Ángeles Unit (∼67 Ma) emplaced at 35°30′S during the first magmatic period (80–59 Ma) (**Figure 2**). This sequence comprises basaltic to andesitic lava flows with interbedded volcanic breccias and lithic sandstones, intruded by basaltic dikes with typical columnar jointing (for a detailed description and stratigraphic columns, see Iannelli et al., 2018). Los Ángeles Unit appears in discordance over Cretaceous marine and non-marine deposits and show changes in dip and thickness along strike, indicating that its deposition was controlled by E-W syn-sedimentary normal faults (**Figure 3**; Fennell et al., 2019). The maximum depositional age of a lithic sandstone interbedded between the lava flows of the Los Ángeles Unit yielded 67.1 + 2.4/-0.9 Ma from U-Pb ages of detrital zircon and agrees with crystallization ages in other volcaniclastic rocks of the region (Fennell et al., 2019 and references therein).

The second studied sequence corresponds to the Eocene Huitrera Formation (Pilcaniyeu Belt) emplaced in the North Patagonian Andes (∼40°S; **Figure 3**) during the second magmatic period (∼59–37 Ma). It comprises bimodal sequences composed of porphyritic lava flows with rhyolitic and basaltic compositions interbedded with pyroclastic facies, such as lithic to vitreous tuffs and conglomerate deposits (Iannelli et al., 2017). The age of the sequence is constrained by a whole-rock Ar–Ar age obtained for a basaltic rock from the basal levels that yielded an age of 44.3 ± 0.13 Ma (Iannelli et al., 2017).

Finally, the last studied sequence corresponds to the Oligocene Auca Pan Formation located at 39°S (**Figure 3**) and associated with the northernmost expression of the El Maitén belt (Rapela et al., 1983). A whole-rock Ar–Ar age from a basaltic rock located in the basal levels of this Formation is 29.6 ± 1.2 Ma (Ramos et al., 2014). This magmatic sequence is composed of basaltic to andesitic lava flows with porphyritic texture with plagioclase, olivine, and clinopyroxene phenocrysts. Locally, lava flows with a thickness of ∼50–100 km grade toward more vesiculated lava facies. Pyroclastic deposits represented mostly by vitreous tuffs are also locally interbedded between lava flows (for details, see Iannelli et al., 2017). The deposition of Auca Pan Formation is controlled by normal faulting causing important variations in strata thickness along the area (Ramos et al., 2014). Locally, the northernmost studied section is controlled by a homoclinal structure with a 35° dip to the east.

Geochemical Features for Studied Late Cretaceous to Oligocene Magmatic Sequences Through Major and Trace Elements Composition

The following chapters summarize the results of the geochemical characterization using published major and trace element data from Los Ángeles Unit (67 Ma; 35°30′S) (Iannelli et al., 2018), Huitrera (44 Ma; 40°30′S), and Auca Pan Formations (29 Ma; 39°40′S) (Iannelli et al., 2017).

Late Cretaceous to Early Paleocene Stage: Los Ángeles Unit

The Late Cretaceous volcanic rocks (Los Ángeles Unit, ∼67 Ma) are composed of basaltic to andesitic lavas with a SiO_2 range between 44.4 and 53.8 wt.%. They are characterized by a subalkaline tholeiitic to alkaline trend (**Figure 4A**) (FeO_t/MgO:1.1–2.9). Fractional crystallization of olivine, clinopyroxene, and Fe-Ti oxides have been recognized as a minor process in the evolution of this sequence (Iannelli et al., 2018). Trace elements classification diagram shows that the Los Ángeles Unit presents a trend between the andesitic/basalt and andesite fields toward the trachy-andesitic one, consistent with major elements classification (**Figure 4B**). When considering the stratigraphic distribution, there is an increase in alkaline composition toward the upper levels of the sequence as can be seen in **Figure 4D**, where the samples display a trend of increasing Ta/Yb ratio at relatively constant Th/Yb. Moreover,

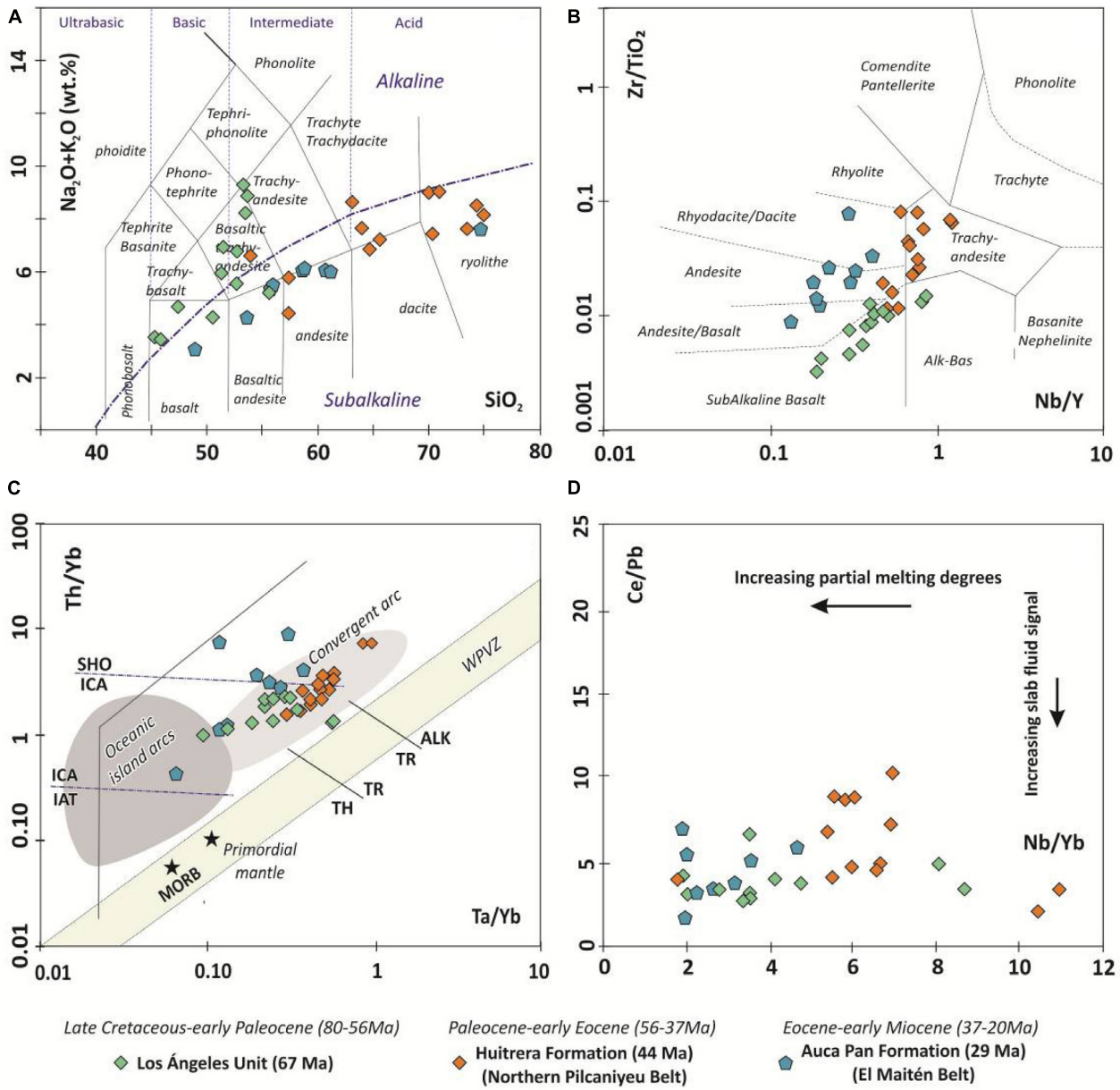

FIGURE 4 | (A) TAS classification diagram for studied Late Cretaceous, Eocene, and Oligocene sequences (Irvine and Baragar, 1971; Le Maitre et al., 1989). **(B)** Trace elements classification plot showing important differences between the three studied sequences. **(C)** Th/Yb vs. Ta/Yb diagram proposed by Pearce (1983) and modified from Xia and Li (2019), which allows constraining a tectonic setting for each studied sequence (SHO, Island arc Shoshonites; ICA, Island arcs Calc-alkaline basalts; IAT, Island arc Tholeiites; TH, Tholeiitic series; TR, Transitional series; ALK, Alkaline series; MORB, Mid-ocean ridge basalts; WPB, Within-plate basalts). **(D)** Ce/Pb vs. Nb/Yb as indicators of partial melting degrees and slab-fluid influence. Geochemical data are from Iannelli et al. (2017, 2018).

the decreasing Ce/Pb and increasing Nb/Yb trends indicate that the slab-fluid signal and partial melting degrees decrease during the magma evolution (**Figure 4D**).

Normalized N-MORB multi-element diagram shows a pronounced enrichment in LILE elements toward the upper magmatic pulses, also partially seen among all the REE elements (**Figure 5A**). This enrichment shows a subduction imprint evidenced by positive anomalies in Rb, Ba, and Th and the depletion in Nb and Ta. However, this sequence is more enriched in Nb, Ta, and REE incompatible elements than the average TSVZ (Transitional Southern Volcanic Zone) and shows, gradually, a similar multi-element pattern to the ocean island basalts (OIB) (**Figure 5A**).

Early Paleocene–Late Eocene Stage: Huitrera Formation

The studied Eocene Huitrera Formation (44 Ma) emplaced at ∼40°S is characterized by a bimodal volcanic sequence

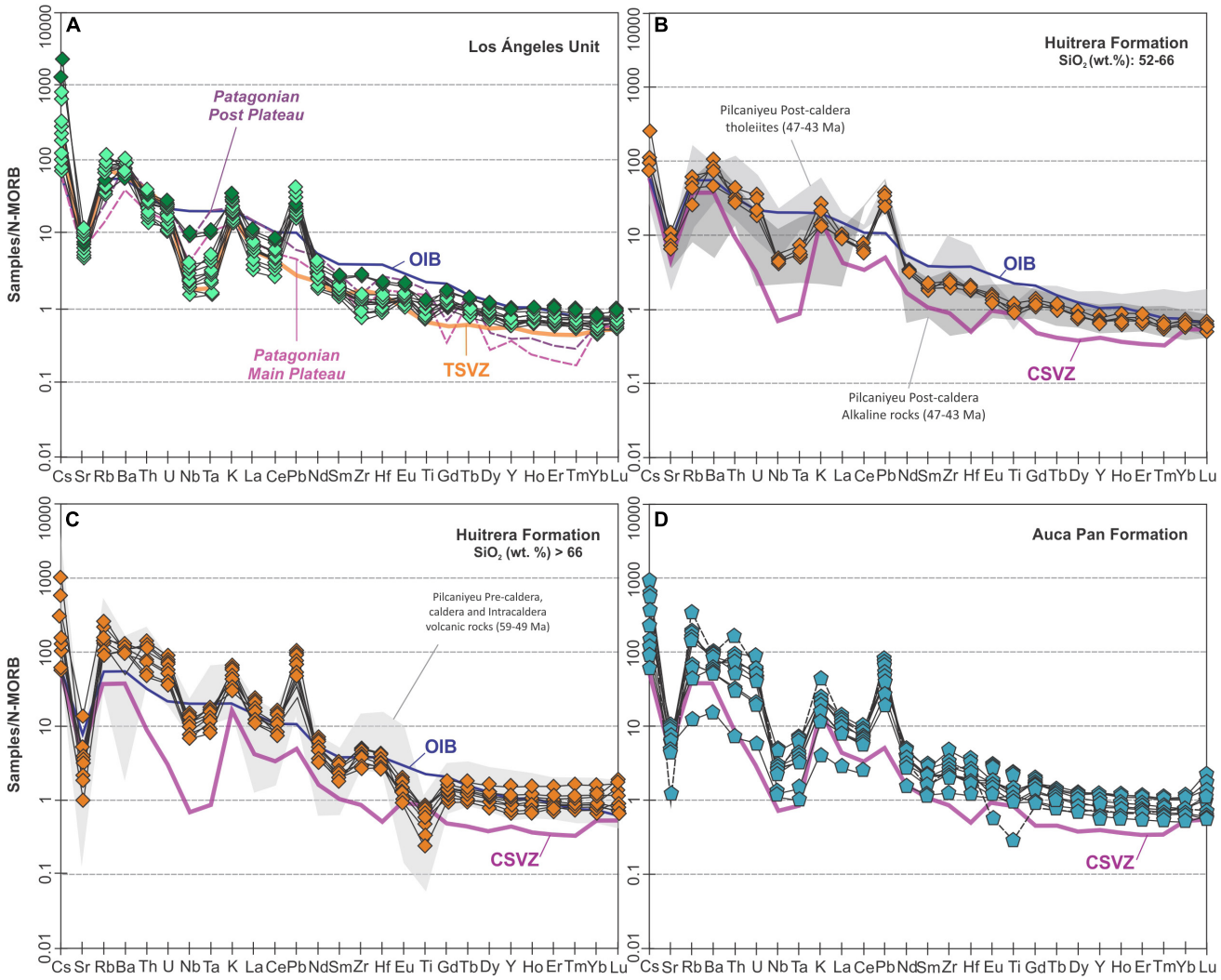

FIGURE 5 | (A) Multi-element diagram for the Late Cretaceous Los Ángeles Unit. **(B,C)** Multi-element diagrams for intermidiate and acid volcanic rocks of Huitrera Formation, respectively. **(D)** Multi-element diagram for the Auca Pan Formation. Geochemical data of the studied sequences are taken from Iannelli et al. (2017, 2018). Average of TSVZ (34.5–38°S) corresponds to Futa and Stern (1988); Hickey-Vargas et al. (1986), Ferguson et al. (1992); Wehrmann et al. (2014), and Jacques et al. (2013). The average of the CSVZ (38–43°S) corresponds to Mella et al. (2005); López-Escobar et al. (1992)López-Escobar et al. (1995); Deruelle (1982), and Wehrmann et al. (2014). The average of the OIB composition is from Sun and McDonough (1989), while the geochemical data for Pilcaniyeu pre-, intra-, and post-caldera stages are from Aragón et al. (2011). Patagonia Main and Post plateau data correspond to the Neogene back-arc magmatism presented by Gorring and Kay (2001).

with basaltic-andesites (SiO_2: 51.6–61.7 wt.%) and rhyolitic compositions (SiO_2:63.8–73.3 wt.%) (**Figure 4A**; Iannelli et al., 2017). When considering major and trace elements classification, a trend toward a transitional signature between subalkaline and alkaline compositions is seen (Nb/Y: 0.5–1.2) (**Figures 4A,B**). The relatively high Ta/Yb, Ce/Pb, and Nb/Yb ratios show a partially lower slab contributions influence and lower melting degrees than the CSVZ (Central Southern Volcanic Zone) composition (**Figures 4B,D**).

N-MORB normalized multi-element diagrams for intermediate (52–66 wt.%) and acid rocks (>66 wt.%) present typical arc-like patterns (e.g., relative depletion in Nb and Ta and enrichment in Rb, Ba, Th, and K). Huitrera Formation at 40°S shows a higher general enrichment in LILE and HFSE when compared to the average CSVZ (38–42°S), close to the OIB composition (**Figures 5B,C**; Sun and McDonough, 1989).

Late Eocene–Early Miocene Stage: Auca Pan Formation

The studied early Oligocene Auca Pan Formation (∼29 Ma; 39°S), associated with the El Maitén Belt (∼40–43°S), is composed of basaltic to andesitic lava flows interbedded with vitreous tuffs. Lava flows show a SiO_2 range between 47.2 and 60.5 wt.%, classifying mostly as subalkaline andesitic to basaltic rocks (**Figures 4A,B**). FeO/MgO ratios are indicative

of a calc-alkaline composition, while trace elements ratios also show a basaltic to andesitic composition (**Figure 4B**). These rocks show a marked arc-like signature, characterized by the high Th/Yb and low Ta/Yb ratios, with significative slab-fluid contributions and high partial melting degrees, as indicated by the low Ce/Pb (1.7–6.9) and Nb/Yb (1.3–4.7) ratios, showing a similar range than CSVZ (38–43°S) (**Figures 4C,D**).

Auca Pan Formation presents a typical arc-like pattern in the multi-element diagram, with similar LILE contents than the CSVZ (38–43°S), although the most evolved samples present more enriched trace element compositions comparable to the UCC average composition (**Figure 5D**; Rudnick and Gao, 2003). Fractional crystallization process has been considered as one of the main mechanisms for controlling the evolution of the Auca Pan Formation sequence, while crustal contamination would have had a minor influence, according to trace elements composition (Iannelli et al., 2017).

METHODOLOGY

Compiled Arc-Like Andean Dataset

To make a regional comparison of the studied arc-related magmatic units along the Andean margin from Late Cretaceous to early Miocene times (∼80–20 Ma), we compiled geochemical data from previous works, based on three main temporal stages. **Figure 6** shows a schematic stratigraphic diagram that represents the coeval arc-related sequences included for the regional comparison in each magmatic stage: (1) For the first one, between Late Cretaceous and early Paleocene times (80–59 Ma), we included magmatism located between 34° and 35°S (Plan de Los Yeuques Formation; 80–63 Ma; Muñoz et al., 2018), arc-related magmatism between 36° and 38°S (Naunauco Group; 74–59 Ma; Zamora Valcarce et al., 2006; Llambías and Aragón, 2011; Mateo-Fernández Caso et al., 2011; Salvioli et al., 2017), and the Late Cretaceous intrusions located along the North Patagonian Cordillera (35–41°S, 94–65 Ma) together with the fore-arc intrusions at the same latitudes mainly emplaced in the Chilean Central Depression (91–80.5 Ma) (Lucassen et al., 2004; De La Fuente, 2014; **Figure 1**). (2) For the second magmatic period, between the Paleocene and the Eocene (59–37 Ma), we included arc-related sequences emplaced between 36° and 38°S (PVNM) (*Provincia Magmática Neuquino Mendocina*; 56-38 Ma; Rapela and Llambías, 1985; Llambías and Rapela, 1989) and magmatism located along the Patagonian Precordillera between 40° and 43°S (Pilcaniyeu magmatic belt; 57–43 Ma) (Rapela et al., 1988; Aragón et al., 2011; Iannelli et al., 2017). (3) For the last magmatic period defined between the latest Eocene to the early Miocene (37–20 Ma) we considered from north to south, the volcanic sequences developed along intra-arc basins mainly located between 33° and 36°S (Abanico Formation; 36–20 Ma; 33–36°S; Kay et al., 2005; Muñoz et al., 2006; Montecinos et al., 2008; Piquer et al., 2017), magmatic units between 36° and 38°S (lower Cura Mallín Formation; 27-20 Ma; 36-39°S; Burns et al., 2006; Kay et al., 2006; Utgé et al., 2009), and the arc-related sequences developed along the Central Depression between 37° and 43.5°S (Coastal Magmatic Belt, CMB; 28–20 Ma; López-Escobar and Vergara, 1997; Muñoz et al., 2000).

We also include for comparison the Southern Volcanic Zone recent magmatism according to the division criteria presented by Jacques et al. (2013, 2014). Thus, for comparing with the studied Los Ángeles Unit (67 Ma; 35°30′S), we considered the quaternary volcanoes between 34.5° and 38°S, grouped as the Transitional Southern Volcanic Zone (TSVZ) (Hickey-Vargas et al., 1986; Ferguson et al., 1992; Futa and Stern, 1988; Wehrmann et al., 2014), whereas for comparisons with the Huitrera (44 Ma; 40°S) and Auca Pan Formations (29 Ma; 39°S), we compare with the magmatic units from the Central Southern Volcanic Zone (CSVZ, 38–43°S) (Deruelle, 1982; López-Escobar et al., 1995, 1992; Mella et al., 2005; Wehrmann et al., 2014).

Isotopic Analysis

New Sr-Nd-Pb isotopic analysis has been made on six basaltic to andesitic lavas from the Los Ángeles Unit (67 Ma, 35°30′S), one basalt and three rhyolites from the Huitrera Formation (44 Ma, Northern Pilcaniyeu Belt, 40°S), and six basaltic to andesitic lavas from the Auca Pan Formation (29 Ma, El Maitén Belt, 39°S). Moreover, three basement rocks from the different areas and temporal stages were also analyzed, which comprises the Choiyoi Group (CHOI1, 35°S) and the metamorphic (PAT3J) and igneous (PAT2J) basement of North Patagonia (39–40°S). Whole-rock Sr, Nd and Pb isotope ratios were obtained through thermal ionization mass spectrometry (TIMS) on a Triton plus instrument (Thermo Scientific) at the Isotope Geochemistry Laboratory of MARUM, University of Bremen (Germany). Sample preparation, mass spectrometric analyses, and external reproducibility of the methods in the Bremen laboratory are documented in Höppner et al. (2018).

Calculation of Tomography Sections

To test the potential existence of slab windows since the Late Cretaceous with an independent methodology, we studied the mantle structure below South America. Recent studies revealed that due to the prolonged times involved in whole mantle convection (>100 Ma), the lower mantle still preserves positions of former subduction configurations back to latest Paleozoic times (van der Meer et al., 2010, 2012). In other words, the current distribution of the lower mantle can be linked to the paleo-subduction zone configuration, which yields coherent correlations of plate reconstructions with mantle structure for the last 300 Ma (van der Meer et al., 2010, 2012, 2018. Here, we combine plate kinematic reconstructions with the mantle structure to locate the ancient positions of potential slab windows (Gianni et al., 2019). A similar approach has been followed in previous studies to map ancient slab windows in North America (Gaina and Jakob, 2019) and Sumatra (Fabian et al., 2010). In South America, a recent study has shown that the oceanic slab at a depth of 1300 km

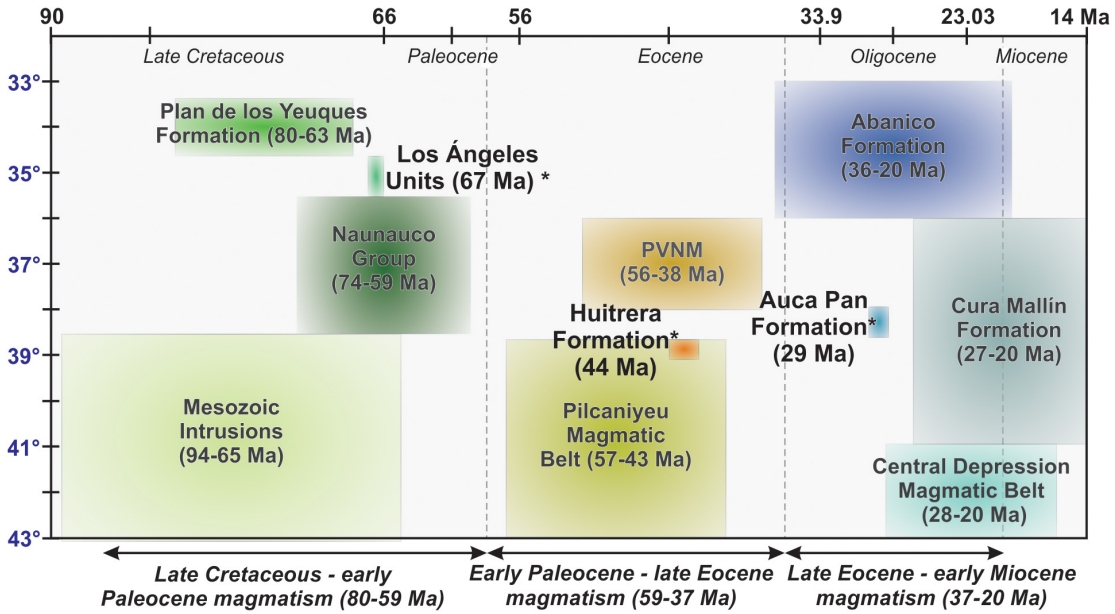

FIGURE 6 | Schematic diagram showing the main arc-related units used in the regional comparison. Geochemical data area from the following: for the first magmatic period (80–59 Ma): Casé et al. (2008); De La Fuente (2014), Franchini et al. (2003); Iannelli et al. (2018), Llambías and Aragón (2011); Lucassen et al. (2004), Mateo-Fernández Caso et al. (2011); Muñoz et al. (2018), and Zamora Valcarce et al. (2006); for the second magmatic period (59–37 Ma): Aragón et al. (2011); Iannelli et al. (2017), Kay et al. (2006), and Llambías and Rapela (1989); and for the last period (37–20 Ma): Iannelli et al. (2017); Kay et al. (2005)Kay et al. (2006); López-Escobar and Vergara (1997), Piquer et al. (2017), and Utgé et al. (2009).

below the Andean margin represents subduction since Late Cretaceous times (Chen et al., 2019). Hence, any relict of the past development of a slab window should be still being visible as a slab gap in the deeper slab (Fabian et al., 2010; Gianni et al., 2018a).

We analyze global P-wave and S-wave seismic tomography models in combination with a recent plate kinematic reconstruction model (Müller et al., 2016) using the Gplates 2.0 software[1]. For our analysis, we used a 1.5 cm/year slab sinking rate that has been previously calculated for the bottom of the subducted Aluk plate (van der Meer et al., 2018). This value is reasonable as it is between average values of 20 cm/year determined from geodynamic modeling (Steinberger et al., 2012) and 1.2 cm/year derived from global slab reconstructions (van der Meer et al., 2010; Shephard et al., 2017). This slab sinking rate was obtained for the study area by correlating the depths of the San Matías slab (i.e., Aluk plate previous to subduction) with the subduction magmatic history beneath Patagonia (van der Meer et al., 2018). This correlation strategy is based on linking slabs to their geological record assuming that slabs tend to sink vertically in the lower mantle, as was recently corroborated by Domeier et al. (2016). We carried out an additional reconstruction considering a slower slab sinking rate of 1.3 cm/year determined for subducted slabs beneath South America (Chen et al., 2019; **Supplementary Figure S1**).

We are aware that although used in many studies, assuming slab sinking vertically and at a constant rate is a simplification as slabs subduct at different rates in upper and lower mantle and can have different geometries, depending on ambient mantle viscosity, slab viscosity, and subduction history (see discussion in Billen, 2008). However, as shown in previous works and the analyses in the following sections, this assumption leads to a good correlation of the mantle structure with the bedrock record. Future studies could focus in reproducing the mantle structure through numerical modeling (e.g., Braz et al., 2018).

To test the existence of a slab window event by Late Cretaceous times, we analyzed the subducted slab with tomography slices from three seismic tomography models (PRI-05; Montelli et al., 2006; GAP-P4, Obayashi et al., 2013; SPani-P, Tesoniero et al., 2015) at a depth of 1200 km (~80 Ma). Then, we searched for a slab gap or along-strike slab discontinuity and compared its position with the hypothetical location of the Farallon–Aluk mid-ocean ridge location derived from Müller et al.'s (2016) reconstruction, which incorporates the ridge kinematics determined by Eagles and Scott (2014). Then, we carried out a finer analysis using the high-resolution UU-P07 global P-wave seismic tomography model (Amaru, 2007). This model has been previously used to build plate reconstructions in the Mesozoic and is generally chosen for analyses like ours (van der Meer et al., 2010; Gianni et al., 2019). We present additional reconstructions for the PRI-05, GAP-P4, and Spani-P models in **Supplementary Figure S2**. In this analysis, we examine the time–space evolution of identified slab gaps to test the correlation with mid-ocean ridge positions from plate kinematic reconstructions and the location of anomalous magmatism attributed to slab window events. For this, we analyzed the subducted slab with tomography

[1]http://www.gplates.org/

slices at a depth of 1250, 850, and 450 km corresponding to the fossil record of subduction in Late Cretaceous (∼80–65 Ma), Paleocene–Eocene (60–50 Ma), and late Eocene–Oligocene times (40–30 Ma).

RESULTS

Isotopic Signature of the Studied Late Cretaceous to Oligocene Magmatic Sequences

Late Cretaceous–Early Paleocene Los Ángeles Unit (67 Ma)

New isotopic data from the Los Ángeles Unit (67 Ma; 35°30′S) comprises basaltic to andesitic lavas from the basal, middle, and upper levels of the sequence and from the basaltic dikes, which are considered the last magmatic pulses of this volcanism (**Table 1**). Los Ángeles Unit volcanic rocks have $(^{87}Sr/^{86}Sr)_i$ ratios ranging from 0.70371 to 0.70496 and $(^{143}Nd/^{144}Nd)_i$ ratios between 0.51260 and 0.51279 (εNd = + 1.02 to + 4.63), plotting alongside the mantle array (**Figure 7A** and **Table 1**). The isotopic variation can be partially correlated with the stratigraphic position of the studied samples, which shows a trend toward a more depleted source in the youngest lavas (**Table 1**). However, the two samples from the basaltic dikes (SVA09-SVA26) present $(^{87}Sr/^{86}Sr)_i$ ratios of 0.70472 and 0.70496 and a $(^{143}Nd/^{144}Nd)_i$ range of 0.512789–0.512757, plotting away from the mantle array toward higher $(^{87}Sr/^{86}Sr)_i$ ratios (**Figure 7A**). High Sr isotopic ratios with positive εNd can be explained by hydrothermal alteration with seawater (e.g., Hofmann and White, 1982), but marine deposits and strong alteration are both absent through the sequence (Iannelli et al., 2018). An overprint of the real isotopic data due to meteoric alteration is the most adequate explanation, which have reduced the Rb/Sr ratios by producing Rb loss and Sr gain causing an under-correction of the initial ratios. $(^{87}Sr/^{86}Sr)_i$ ratios would be overestimated as the Sr and Rb (ppm) values used for recalculating the initial isotopic ratios might have been altered (e.g., Plimer and Elliott, 1979).

The general isotopic signature seen in the Late Cretaceous–early Paleocene Los Ángeles Unit contrasts with the isotopic values for the local basement corresponding to the Choiyoi Group (CHOI1), which presents higher $(^{87}Sr/^{86}Sr)_i$ and lower $(^{143}Nd/^{144}Nd)_i$ ratios consistent with the Paleozoic basement rocks (**Figure 7A** and **Table 1**; Lucassen et al., 2004).

Los Ángeles Unit rocks show $^{206}Pb/^{204}Pb$ = 18.40–18.57, $^{207}Pb/^{204}Pb$ = 15.51–15.57, and $^{208}Pb/^{204}Pb$ = 38.04–38.33 (**Table 1**). Most of the samples show Pb isotopic signatures similar to the isotopic compositional field for the depleted MORB (**Figures 8A,B**). No correlation between Pb isotopic composition and the stratigraphic position of the samples is seen (**Table 1**). Los Ángeles Unit presents a partially higher $^{206}Pb/^{204}Pb$ and $^{208}Pb/^{204}Pb$ ratios than the local basement represented by the Choiyoi Group sample (CHOI1) (**Figures 8A,B** and **Table 1**). Considering the plumbotectonic model from Zartman and Doe (1981), Pb isotopic composition varies between the mantle growth curve and the orogen growth curve, for both the uranogenic and the thorogenic Pb (**Figures 8A,B**).

Eocene Huitrera Formation (44 Ma)

The Eocene Huitrera Formation volcanism (∼44 Ma; 40°S) presents $(^{86}Sr/^{87}Sr)_i$ ratios between 0.70399 and 0.70411, with $(^{143}Nd/^{144}Nd)_i$ ratios between 0.51267 and 0.51274 (εNd: + 1.76– + 3.10) (**Table 1**). Therefore, Eocene rocks are distributed along the mantle array, showing higher $(^{86}Sr/^{87}Sr)i$ and lower εNd values than the average depleted mantle composition (**Figure 7B**). However, one sample (DP49) shows a remarkably higher $(^{87}Sr/^{86}Sr)_i$ ratio of 0.70692 but with a similar εNd value, plotting outside the mantle array that could be associated with seawater alteration (**Figure 7B**). As a marine environment has not been described for the emplacement of this sequence, we considered that the high $(^{87}Sr/^{86}Sr)_i$ ratio is caused by meteoric alteration, which would have disturbed Rb/Sr ratios and so the under-correction of the initial isotopic ratios [see discussion in section Late Cretaceous- Early Paleocene Los Ángeles Unit (67 Ma)]. Thus, a reliable $(^{87}Sr/^{86}Sr)_i$ ratio cannot be calculated for this sample as it shows plagioclase altered to epidote and sericite, and so Sr content might have been affected by meteoric fluids (e.g., Plimer and Elliott, 1979). We dismiss its $(^{87}Sr/^{86}Sr)_i$ values from the final interpretation, although Nd and Pb isotopic ratios can still be reliable.

Sr and Nd isotopic composition of Huitrera Formation samples clearly differentiate from the two samples of the metamorphic and intrusive Paleozoic basement at the North Patagonian Andes (samples PAT2J and PAT3J) that plot outside the limits of **Figure 7C** at considerably high Sr ratios and low ε Nd.

Huitrera Formation Pb isotopic composition is presented in **Table 1**. This volcanic sequence shows $^{206}Pb/^{204}Pb$ = 18.49–18.61, $^{207}Pb/^{204}Pb$ = 15.53–15.59, and $^{208}Pb/^{204}Pb$ = 38.22–38.47 values, plotting along the orogenic growth curve (Zartman and Doe, 1981). The isotopic signature of studied Eocene volcanism is partially similar to the local basement samples (PAT2J and PAT3J) (**Figures 8C,D**).

Oligocene Auca Pan Formation (29 Ma)

The Oligocene Auca Pan Formation (∼29 Ma; 39°S) is characterized by initial $^{86}Sr/^{87}Sr$ ratios between 0.70397 and 0.70486 and $(^{143}Nd/^{144}Nd)$ and between 0.51267 and 0.51275 (εNd: + 1.37– + 2.99) (**Table 1**). According to **Figure 7C**, Oligocene rocks show increasing initial $^{87}Sr/^{86}Sr$ ratios for a limited initial $^{143}Nd/^{144}Nd$ and ε Nd range.

The two samples that represent the metamorphic and intrusive Paleozoic basement at the North Patagonian Andes were included for comparison (samples PAT2J and PAT3J), showing considerably higher Sr ratios and lower εNd than Auca Pan Formation (**Figure 7C**).

Auca Pan Formation lavas show the following isotopic lead ratios: $^{206}Pb/^{204}Pb$ = 18.53–18.72, $^{207}Pb/^{204}Pb$ = 15.53–15.65, $^{208}Pb/^{204}Pb$ = 38.27–38.72 (**Table 1**). Pb isotope ratios in Oligocene volcanism are similar to those of the underlying basement represented by the samples PAT2J and PAT3J, although

TABLE 1 | Initial Sr, Nd, Pb isotope ratioscalculated from the measurements of the current isotope ratios (TIMS), and Rb, Sr, Sm, Nd, U, Th, Pb element concentration of whole rock samples.

Sample	Rb (ppm)	Sr (ppm)	$^{87}Sr/^{86}Sr \pm 2\sigma$	$(^{87}Sr/^{86}Sr)_i$	Sm (ppm)	Nd (ppm)	$^{143}Nd/^{144}Nd \pm 2\sigma$	$(^{143}Nd/^{144}Nd)_i$	eNd	U (ppm)	Th (ppm)	Pb (ppm)	$^{206}Pb/^{204}Pb$	$^{207}Pb/^{204}Pb$	$^{208}Pb/^{204}Pb$
LATE CRETACEOUS LOS ÁNGELES UNIT (67 Ma)															
SVA09	55	260	0.7053 ± 5	0.704716	6.9	31.2	0.512847 ± 7	0.512789	4.6	1.2	3.5	12	18.43	15.56	38.19
SVA26	37	574	0.705136 ± 7	0.704958	6.3	28.6	0.512815 ± 8	0.512756	3.9	1	3	16	18.5	15.61	38.48
SVA13	42	493	0.703993 ± 6	0.703757	3.8	16.2	0.512767 ± 5	0.512704	2.9	0.6	1.7	6	18.54	15.58	38.35
SVA17	45	555	0.704094 ± 4	0.703871	5.2	23	0.512663 ± 18	0.512603	1.1	1.2	4.3	11	18.58	15.58	38.42
SVA10	28	592	0.703837 ± 5	0.703707	4.5	19.3	0.512739 ± 7	0.512677	2.4	1.1	3.5	12	18.56	15.58	38.38
SVA28	19	470	0.703818 ± 4	0.703707	3.9	13.8	0.512717 ± 7	0.512642	1.8	0.6	2.1	< 5	18.53	15.58	38.36
SVA30	21	574	0.704306 ± 7	0.704205	3.5	12.6	0.512724 ± 6	0.512651	1.9	1.2	3.9	8	18.6	15.61	38.48
EOCENE HUITRERA FORMATION (44 Ma)															
DP41	77	241	0.704691 ± 8	0.704109	6.7	33.2	0.512744 ± 6	0.512708	2.5	2.63	10.4	16	0	0	0
DP49	91	144	0.708067 ± 10	0.706916	5.6	30.1	0.512708 ± 7	0.512675	1.8	2.61	10.5	8	18.56	15.61	38.49
DP51	113	126	0.70574 ± 5	0.7041068	5.6	29.3	0.512704 ± 5	0.512671	1.7	2.64	11	7	18.57	15.63	38.6
SA10	127	157	0.705801 ± 6	0.703988	4.8	28.2	0.512758 ± 6	0.512721	2.9	3.29	15.3	18	18.64	15.62	38.62
DP58	33	884	0.704223 ± 6	0.704155	5.5	27.5	0.512775 ± 6	0.512739	3.1	1.6	5.15	8	18.52	15.57	38.37
OLIGOCENE AUCA PAN FORMATION (29 Ma)															
AU01	25	854	0.704901 ± 8	0.704865	3.9	19.4	0.512711 ± 6	0.512687	1.7	4.06	11.3	24	18.76	15.69	38.87
AU06	91	408	0.704865 ± 5	0.704598	6.8	34.9	0.512693 ± 8	0.512671	1.4	2.27	9.49	12	18.67	15.65	38.7
AU09	89	401	0.704927 ± 6	0.704662	6.9	33.9	0.512726 ± 4	0.512702	1.9	2.01	8.51	13	18.63	15.59	38.5
AU12	39	463	0.704071 ± 5	0.703968	5.8	23.2	0.512724 ± 6	0.512694	1.8	0.95	3.82	6	18.57	15.61	38.53
AU15	82	486	0.704273 ± 6	0.704067	5.4	27.3	0.512777 ± 8	0.512754	2.9	1.82	6.67	14	18.58	15.59	38.47
AU21	100	481	0.704626 ± 7	0.704373	5.3	26.1	0.512719 ± 6	0.512695	1.8	2.64	8.64	17	18.59	15.57	38.42

Element concentrations by ICP-MS, corresponds to Iannelli et al. (2017, 2018).

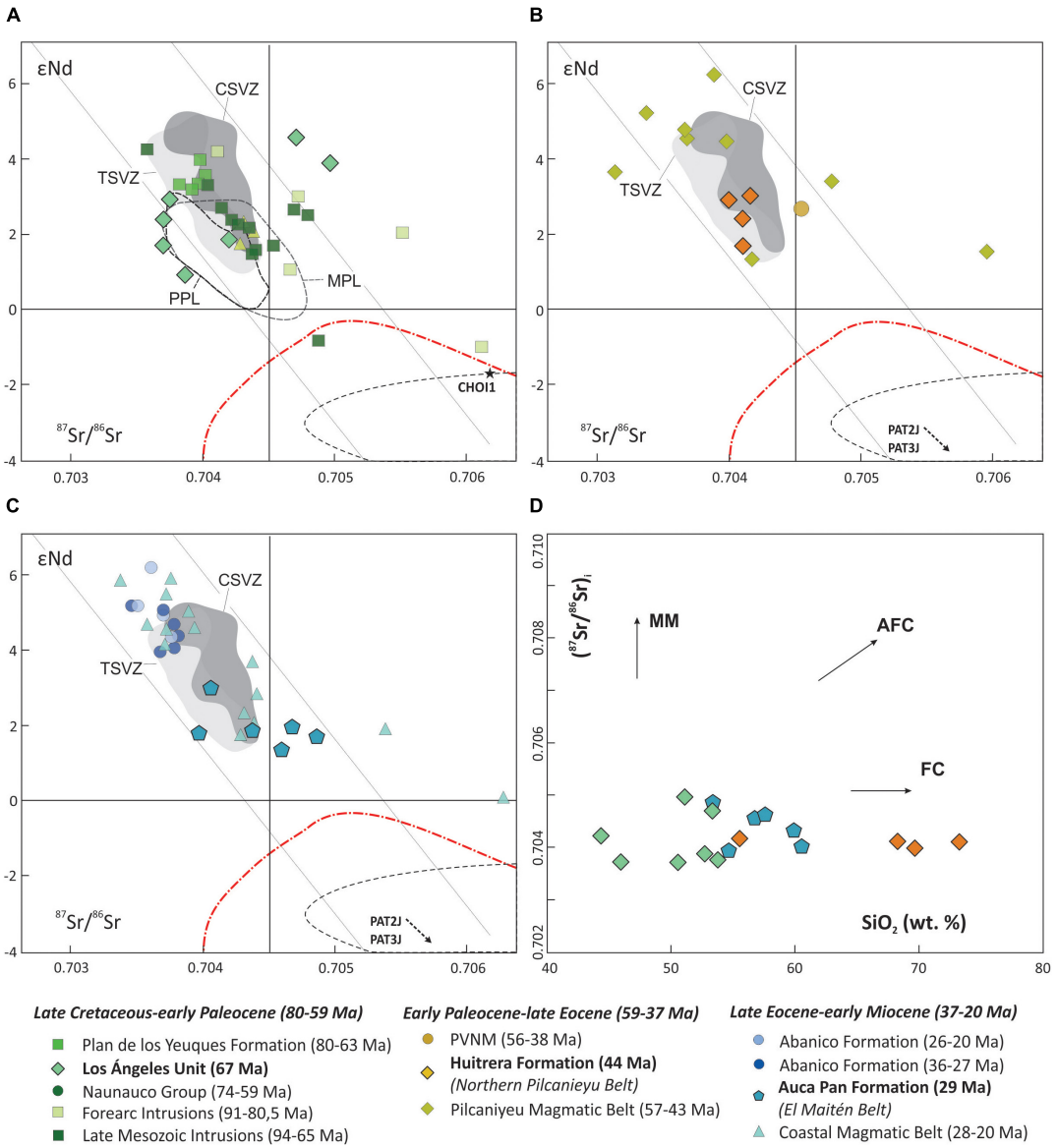

FIGURE 7 | Initial isotopic compositions for Los Ángeles Unit **(A)**, Huitrera Formation **(B)**, and Auca Pan Formation **(C)**. Recalculated initial isotopic ratios from coeval magmatic units are also included. CHOI1 corresponds to the Choiyoi Group considered as the local basement of the Los Angeles Unit area (35°30′S), while PAT2J and PAT3J correspond to the Late Paleozoic metamorphic and igneous local basement of the Huitrera and Auca Pan Formation in the North Patagoniana Andes (39–41°S). The black dashed line corresponds to the Southern Coastal Batholith 30–38°S (Parada et al., 1988; Lucassen et al., 2004), while the red dashed line corresponds to the Metamorphic basement and Late Paleozoic intrusions that represent the Pz basement of the region (Lucassen et al., 2004; Pankhurst et al., 2006). The Transitional Southern Volcanic Zone (TSVZ) isotopic data are from Mella et al. (2005) while Central Southern Volcanic Zone (CSVZ) data are taken from López-Escobar et al. (1992, 1995). The acronyms PPL and MPL correspond to post-plateau lavas and main-plateau lavas that represent the Neogene Patagonian slab window lavas studied by Gorring and Kay (2001). **(D)** $^{87}Sr/^{86}Sr$ vs. SiO_2 (wt.%) showing the AFC (assimilation and fractional crystallization), FC (fractional crystallization), and MM (mantle metasomatism) trends.

the local basement presents higher Pb isotopic compositions (**Figures 8E,F**; Lucassen et al., 2004).

Tomographic and Plate Kinematic Analyses

We begin with an analysis of the mantle structure at depths corresponding to the Late Cretaceous with the specific aim to test the existence of a potential slab window event at this time north of 35°30′–36°S (Iannelli et al., 2018). For this end, we analyzed tomography slices at a depth of 1200 km from global P-wave (PRI-05; Montelli et al., 2006; GAP-P04, Obayashi et al., 2013) and S-wave (SPani-P, Tesoniero et al., 2015) seismic tomography models showing the mantle structure corresponding to subduction at 80 Ma and representing the general subduction evolution in Late Cretaceous between ∼80 and 70 Ma. As seen in **Figure 9** in striking coincidence with

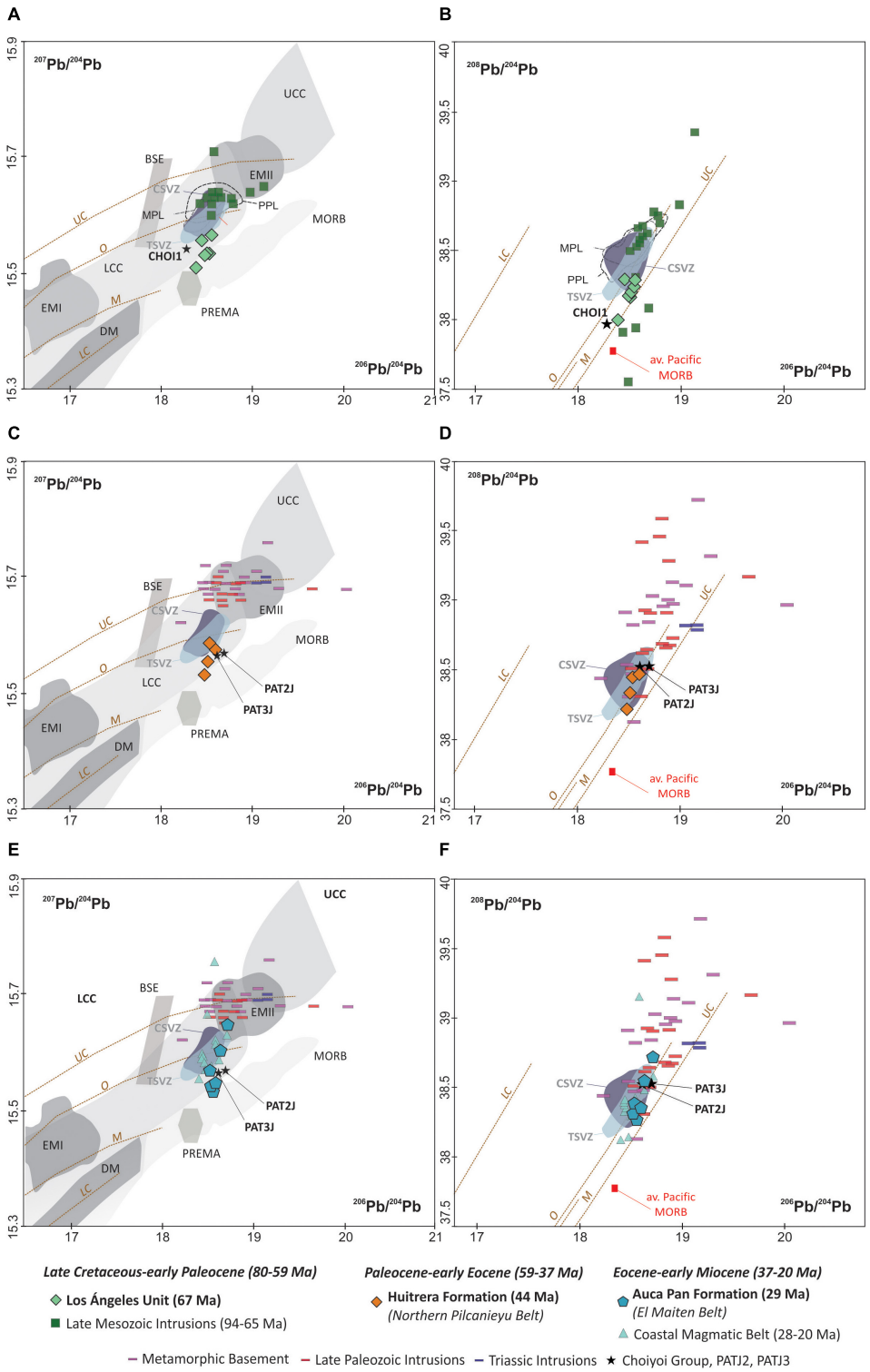

FIGURE 8 | Pb isotopic composition for the Late Cretaceous–early Paleocene Los Ángeles Unit **(A,B)**, the Eocene Huitrera Formation **(C,D)** and the Oligocene Auca Pan Formation **(E,F)**. The fields of the isotopic composition of the different mantle reservoirs are as in Zindler and Hart (1986): upper and lower continental crust (UCC and LCC), depleted mantle (DM), bulk silicate earth (BSE), mantle with high U/Pb ratio (HIMU), enriched mantle I (EMI), enriched mantle II (EMII), and observed prevalent mantle composition (PREMA). Moreover, we also included the isotopic composition of mid-ocean ridge basalt (MORB) and the average Pacific MORB from Lucassen et al. (2001), Neogene Patagonian main and post-plateau lavas from Gorring and Kay (2001), and the compositional fields for the TSVZ and CSVZ from López-Escobar et al. (1992, 1995) and Mella et al. (2005). Figures also include the lead-isotope evolution curves from the plumbotectonic model presented by Zartman and Doe (1981) for the mantle (M), the orogen (O), the upper crust contributed to the orogen (UC), and the lower crust contributions to the orogen (LC).

the area of anomalous magmatism, attributed to a slab window (Iannelli et al., 2018), and the position of the Farallon–Aluk mid-ocean ridge, reconstructed in the plate kinematic model (Müller et al., 2016), a slab gap is clearly observed between 35°S and 30°S in the seismic tomography model. The position of this slab gap in Late Cretaceous is roughly coincident with the analysis of Chen et al. (2019) that locates the southern tip of the Farallon slab at the same latitudes coinciding with the subducted mid-ocean ridge. Also, the inexistence of a slab gap in the inferred triple junction location in the study of Somoza et al. (2012) at 22°S in the Late Cretaceous allows discarding a slab window origin for deformation and magmatism interpreted by those authors (**Figure 10A**). These reconstructions also show that a subducting slab is present beneath Patagonia, south of the Farallon–Aluk ridge (**Figure 9**). The latter is consistent with the presence of significant Late Cretaceous subduction-related magmatism at those latitudes (e.g., Gianni et al., 2018a), and contrasts with the results of Chen et al. (2019).

Furthermore, this slab gap migrated southward along the active Andean margin between Late Cretaceous to Oligocene times following the reconstructed position inferred from plate kinematic reconstructions (Cande and Leslie, 1986; Eagles and Scott, 2014) and slab window-related magmatism (Ramos and Kay, 1992; Aragón et al., 2011; Iannelli et al., 2018; **Figure 10**). This is also illustrated by the southward propagation of subduction initiation between 80–70 and 30 Myr (**Figures 10B,C**). We note that this evolution is not as clear in the Spani-P as this model does not show an evident slab gap at 60 Ma (900 km at Central Patagonian latitudes) (**Supplementary Figure S2**). However, as the slab gap in this model is present at 80 Ma (1200 km, **Figure 9**) and reappears at 30 Ma (450 km, **Supplementary Figure S2**) at the southern extreme of South America, it likely just indicates a lack of resolution of the model at 900 km. With this analysis, we complement the previous study of Chen et al. (2019), which identified a southward propagation of subduction only up to 38–40°S. An additional reconstruction in **Supplementary Figure S1** considering a slower slab sinking rate of 1.3 cm/year (Chen et al., 2019) still indicate the presence of a slab gap at this time, but slightly shifted southward with respect to previous reconstruction in **Figure 10**. However, this reconstruction presents a faster propagation of subduction onset to the south that is fully completed at ∼50 Ma. The latter is not consistent with geological constraints indicating a full active margin magmatism after 40 Ma (Iannelli et al., 2017; Fernández Paz et al., 2018, 2019; Gianni et al., 2018b).

DISCUSSION

Geochemical Evolution of the Studied Arc-Related Magmatic Units From Late Cretaceous to Late Oligocene

Late Cretaceous Los Ángeles Unit Magmatism (35°30′S)

The Latest Cretaceous magmatism of the Los Ángeles Unit (67 Ma; 35°30′S), emplaced during the first studied magmatic period (80–59 Ma), is represented by basaltic to andesitic lava flows intruded by basaltic dikes and controlled by extensional faulting. Lava flows show a transitional subalkaline–tholeiitic to alkaline composition and a decreasing arc-like signature and partial melting degrees toward the younger lavas (**Figures 4**, **11A,B**; Iannelli et al., 2018). Enrichment in incompatible elements is also seen upward in the sequence, associated with possible crustal contamination and/or the input from a more LILE-enriched portion of the mantle (Iannelli et al., 2018).

New isotopic data suggest the contribution of a more pristine and depleted source toward the upper levels of the sequence considering the increasing εNd values from + 1.02 to + 4.63 (**Figure 7A**), also consistent with trace elements behavior (**Figures 4A,B**, **5A**). Los Ángeles Unit isotopic composition is concentrated between the fields of the OIB and the TSVZ, although the last one is even more isotopically depleted (Sun and McDonough, 1989; Gorring and Kay, 2001). Although the Sr isotopic values of the basaltic dikes, considered as the youngest magmatic pulses (SVA09 and SVA26) cannot be used for interpretation (see discussion in section Isotopic Signature of the Studied Late Cretaceous to Oligocene Magmatic Sequences), the Sr isotopic range for the rest of the sequence indicates no evidence in favor of crustal contamination when comparing with the local basement isotopic composition (CHOI1).

Pb isotopes have always been used as indicators of crustal components as this element is highly concentrated in the crust. In particular, Los Ángeles Unit magmatism shows a Pb isotopic range consistent with the depleted MORB isotopic composition (**Figures 8A,B**; Zindler and Hart, 1986). Higher mantle influence is also reflected since these lavas plot nearer the mantle growth curve (Zindler and Hart, 1986). The local basement sample (CHO1) presents lower $^{206}Pb/^{204}Pb$ and $^{208}Pb/^{204}Pb$ ratios and a partially lower $^{207}Pb/^{204}Pb$ ratio, which indicates that this local basement had no influence on the composition of Los Ángeles Unit magmatism (**Figures 8A,B**).

Overall, the new results presented in this work dismissed the incorporation of crustal contributions as the main cause for the enrichment in LILE seen in Los Ángeles Unit, and allow to consider the participation of a more enriched magmatic source as a plausible explanation for its evolution.

Eocene Huitrera Formation Magmatism (40°S)

The second magmatic period (59–34 Ma) is represented by the Huitrera Formation (∼44 Ma) (Northern Pilcaniyeu Belt) composed of rhyolitic and basaltic andesitic lavas interbedded with vitreous and lapillitic tuffs (Iannelli et al., 2017). A transitional alkaline signature associated with a retroarc setting is seen together with minor slab-fluid influence and also minor partial melting degrees (**Figures 4**, **11C,D**; Iannelli et al., 2017).

The new isotopic data for Huitrera Formation shows positive εNd values (1.76–3.10) for a limited $(^{87}Sr/^{86}Sr)_i$, which plot range along the mantle array, with a partially similar enriched composition as the OIB field. When considering Huitrera Formation isotopic behavior relative to the local basement, the latter shows considerably higher $(^{87}Sr/^{86}Sr)_i$ ratios and negative εNd (**Figure 7B** and **Table 1**). Thus, assimilation of the local basement continental crust should have been negligible.

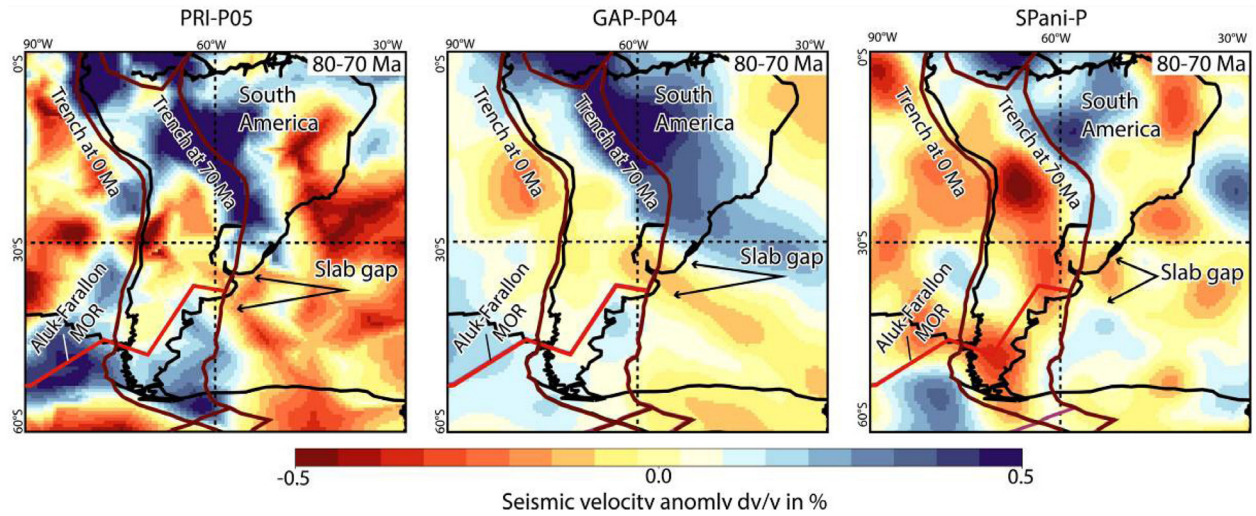

FIGURE 9 | Tomography slices at a depth of 1200 km from global P-wave (PRI-05; Montelli et al., 2006; GAP-P04, Obayashi et al., 2013) and S-wave (SPani-P, Tesoniero et al., 2015) seismic tomography models showing the mantle structure corresponding to subduction in Late Cretaceous (~80–70 Ma).

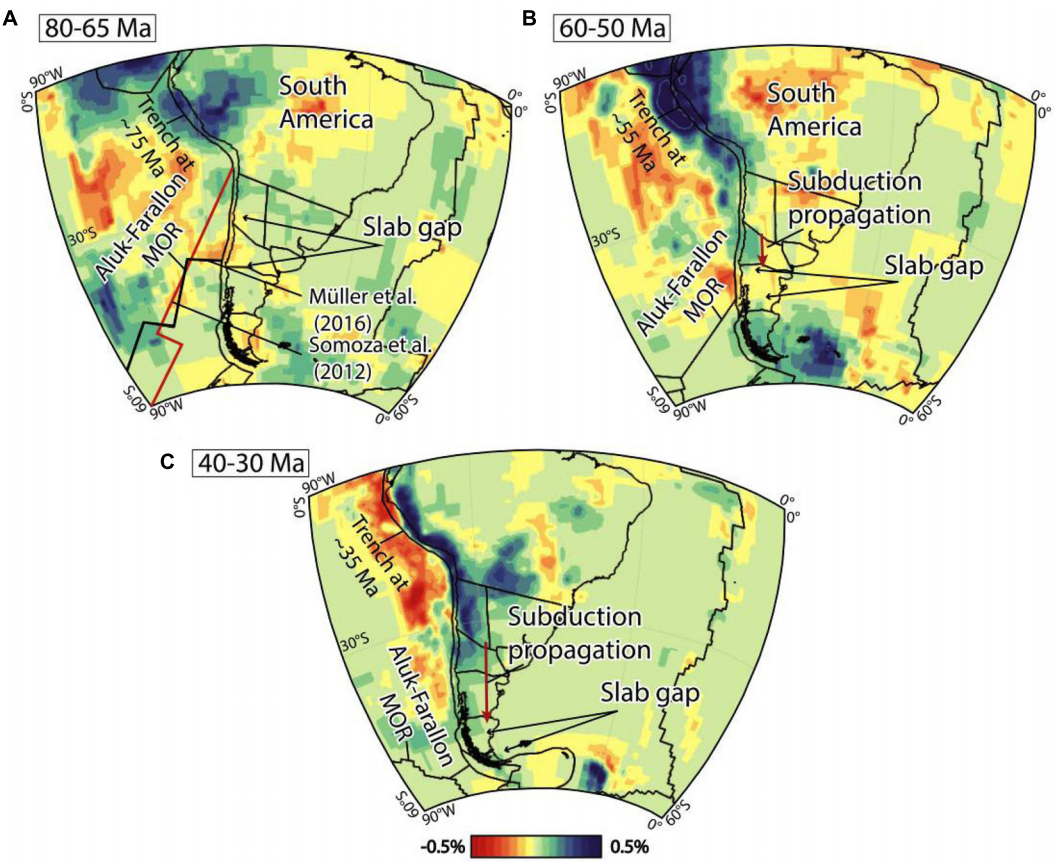

FIGURE 10 | Tomography slices at a depth of **(A)** 1200 km, **(B)** 850 km, and **(C)** 450 km from the UU-P07 global P-wave seismic tomography model (Amaru, 2007). These depths represent three stages of Andean subduction where the preserved mantle structure would correspond to the fossil record of subduction in Late Cretaceous (~80–65 Ma), Paleocene–Eocene (60–50 Ma), and late Eocene–Oligocene times (40–30 Ma), respectively. This image shows a striking coincidence between the southward migrations of a slab gap inferred from a discontinuity in fast anomalies below the Andean margin and the inferred position of the Farallon–Aluk mid-ocean ridge (MOR) from plate kinematic reconstructions (Cande and Leslie, 1986; Eagles and Scott, 2014; Müller et al., 2016).

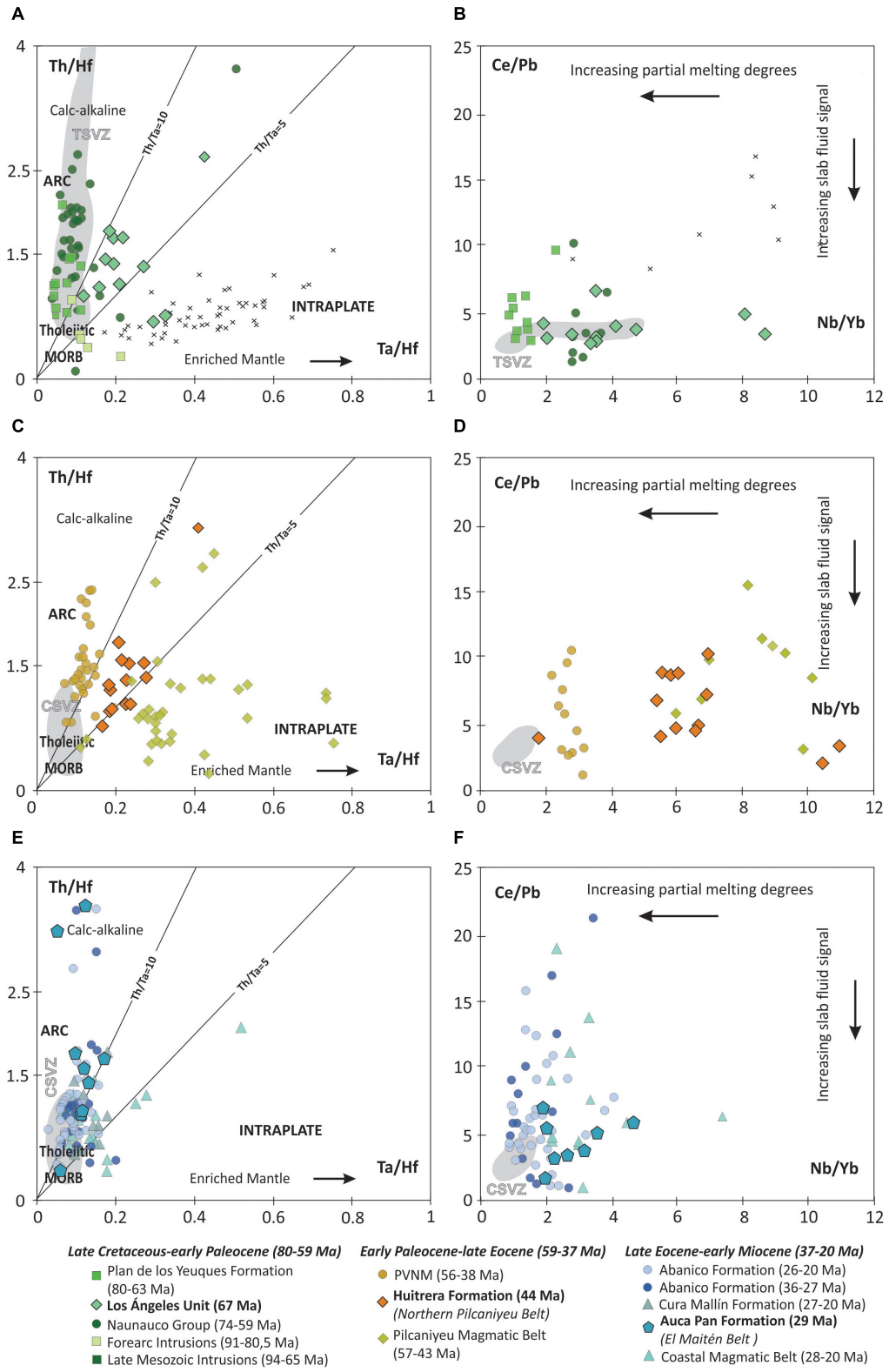

FIGURE 11 | (A,B) Th/Hf vs. Ta/Hf and Ce/Pb vs. Nb/Yb for Late Cretaceous-early Paleocene magmatic units along the Southern Central Andes. **(C,D)** Th/Hf vs. Ta/Hf and Ce/Pb vs. Nb/Yb for early Paleoceno-late Eocene magmatic units along the Southern Central Andes. **(E,F)** Th/Hf vs. Ta/Hf and Ce/Pb vs. Nb/Yb for late Eocene-early Miocene magmatic units along the Southern Central Andes. Gray crosses correspond to the Neogene Main and Post-Plateau lavas from Patagonia retroarc (Gorring and Kay, 2001; Guivel et al., 2006). For references to the data sources, see details in the text (references in section Compiled Arc-Like Andean Dataset). TSVZ corresponds to the Transitional Southern Volcanic Zone (34.5–38°S) while CSVZ corresponds to the Central Southern Volcanic Zone (38–43°S) (references in section Compiled Arc-Like Andean Dataset).

Pb isotopic signature for the Huitrera Formation samples indicates almost similar values for all the samples with almost similar $^{207}Pb/^{204}Pb$ ratios than the basement samples (PAT2J and PAT3J) and a tendency toward the Paleozoic metamorphic and intrusive basement of the North Patagonian Andes (**Figures 8C,D**; Lucassen et al., 2004). This tendency is in favor with the minor amounts of crustal contamination considered for $(^{87}Sr/^{86}Sr)_i$ vs. εNd values. The new isotopic dataset together with previously published major and trace elements composition indicate a partially enriched mantle source for this bimodal magmatic sequence, while crustal contamination could only have a minor influence in its evolution.

Oligocene Auca Pan Formation Magmatism (39°S)

The basaltic to andesitic lavas and pyroclastic rocks of the Auca Pan Formation (29 Ma; Ramos et al., 2014; Iannelli et al., 2017) present a calc-alkaline composition with a typical arc-like behavior and significant slab-fluid contributions associated with high partial melting degrees (**Figures 4**, **11E,F**; Iannelli et al., 2017).

Auca Pan Formation shows variable $(^{87}Sr/^{86}Sr)_i$ with little variation in most εNd (**Figure 7C**). The Sr isotopic signature of studied lava flows is lower than the analyzed basement samples (PAT2J and PAT3J), which might indicate a minor involvement of the local continental crust during magma evolution (**Figure 7C**).

Variable $^{207}Pb/^{204}Pb$ and $^{208}Pb/^{204}Pb$ isotopic ratios are seen for the Oligocene Auca Pan Formation lavas, with an almost constant $^{206}Pb/^{204}Pb$. The most radiogenic samples present similar Pb isotopic values as the local basement (PAT2J and PAT3J), reaching the Paleozoic metamorphic and intrusive basement field (**Figures 8E,F**; Lucassen et al., 2004). Sr, Nd, and Pb isotopic composition of the Auca Pan Formation is in agreement with the clear arc-like signature seen through its major and trace elements composition also revealing minor crustal assimilation.

Regional Comparison of Arc-Related Magmas From the Southern Central to North Patagonian Andean (35–42°S)

Late Cretaceous–Early Paleocene Magmatic Evolution

Late Cretaceous–early Paleocene arc-related magmatism (80–59 Ma) presents a scattered distribution with contrasting geochemical signatures and important magmatic gaps (∼35–42°S, **Figure 1**). Different magmatic units have been recognized along the Southern Central Andes (**Figures 1**, **6**), which are now compared with the studied Los Ángeles Unit magmatism in order to track main geochemical variations along space (**Figures 1**, **6**). From north to south, Late Cretaceous–early Paleocene magmatism is described at 34°30′S named as Plan de Los Yeuques Formation (∼80–63 Ma; Tapia, 2015; Muñoz et al., 2018; Mosolf et al., 2019). Southwards, arc-related sequences have been recognized at 36–38°S, gathered into the Naunauco Group (74–59 Ma; Franchini et al., 2003; Zamora Valcarce et al., 2006; Casé et al., 2008; Llambías and Aragón, 2011; Mateo-Fernández Caso et al., 2011; Salvioli et al., 2017; Iannelli et al., 2018), together with a series of Late Mesozoic intrusions emplaced between 36° and 41°S between the fore-arc and arc zone along the North Patagonian Andes and the Chilean Central Depression (94–65 Ma; Munizaga et al., 1988; Lucassen et al., 2004; De La Fuente et al., 2012, De La Fuente, 2014; **Figures 1**, **6**).

In particular, the geochemical signature of the studied Late Cretaceous Los Ángeles Unit (67 Ma; 35°30′S) shows an increasing alkaline tendency with decreasing arc-like signatures and decreasing partial melting degrees (Iannelli et al., 2018). The enrichment in incompatible elements, together with a change toward a more isotopically depleted signature in the youngest lava flows, suggest a possible change in the magmatic source of the Los Ángeles volcanism.

Northwards (∼34°30′S), Latest Cretaceous magmatic rocks (Plan de Los Yeuques Formation; ∼80–63 Ma) have been recognized in a westward position with respect to the studied Los Ángeles Unit (35°30′S), which present a higher arc-like signature, as seen by their higher Th/Hf, Th/Yb and La/Ta ratios (**Figures 11A**, **12A**). The lower Nb/Yb and Nb/Y ratios of this northern sequence also indicate higher partial melting degrees when compared to the Los Ángeles Unit (**Figures 7B**, **14B**). Isotopic composition shows higher εNd and partially higher $^{87}Sr/^{86}Sr$ ratios for the northern magmatism (34°30′S) relative to the studied Los Ángeles Unit (67 Ma, 35°30′S) (**Figure 7A**).

Southwards (36–41°S), Late Cretaceous–early Paleocene magmatism is characterized by granitic intrusions located in a forearc to arc position with ages between 94 and 65 Ma (**Figure 1**). Geochemical variations are seen between these partially coeval magmatic sequences (36–41°S) and the Los Ángeles Unit (35°30′S). First of all, fore-arc intrusions (∼91–80.5 Ma; 39–40°S) present a calc-alkaline composition with a peraluminous signature seen in their partially high La/Ta ratios, although they present similar Ta/Hf ratios to the Los Ángeles Unit. They show a similar $(^{143}Nd/^{144}Nd)_i$ range to the Los Ángeles Unit but with increasing $(^{87}Sr/^{86}Sr)_i$ ratios that have been associated with possible contamination with the basement rocks (**Figures 11A**, **B**). Some of these rocks show an adakitic imprint, which has been related to a possible slab window during the Late Cretaceous (De La Fuente, 2014). On the other hand, partially eastern coeval Late Mesozoic magmatic intrusions (94–65 Ma; 36–40°S), consist of subalkaline gabbroic to granitic mantle-derived rocks. They present a similar range of εNd than the Los Ángeles Unit but higher $(^{87}Sr/^{86}Sr)_i$ values, suggesting small crustal contributions (**Figure 7A**) and a typical arc-like geochemical imprint (**Figures 11A,B**, 12).

In an eastward position relative to the Late Mesozoic magmatic intrusions, between 36° and 38°S, coeval magmatism (Naunauco Group) is represented by arc-like andesitic rocks with a calc-alkaline composition emplaced during an extensional phase in Andean evolution (Zamora Valcarce et al., 2006; Casé et al., 2008; Llambías and Aragón, 2011). They present higher slab-fluid signal and partial melting degrees than the Los Ángeles Unit (35°30′S), although both of them share a similar retroarc position (**Figures 11A,B**, 12A,B).

Overall, variable geochemical features have been identified in these coeval magmatic units. A predominance of arc-like compositions is seen along the Southern Central Andes, mainly

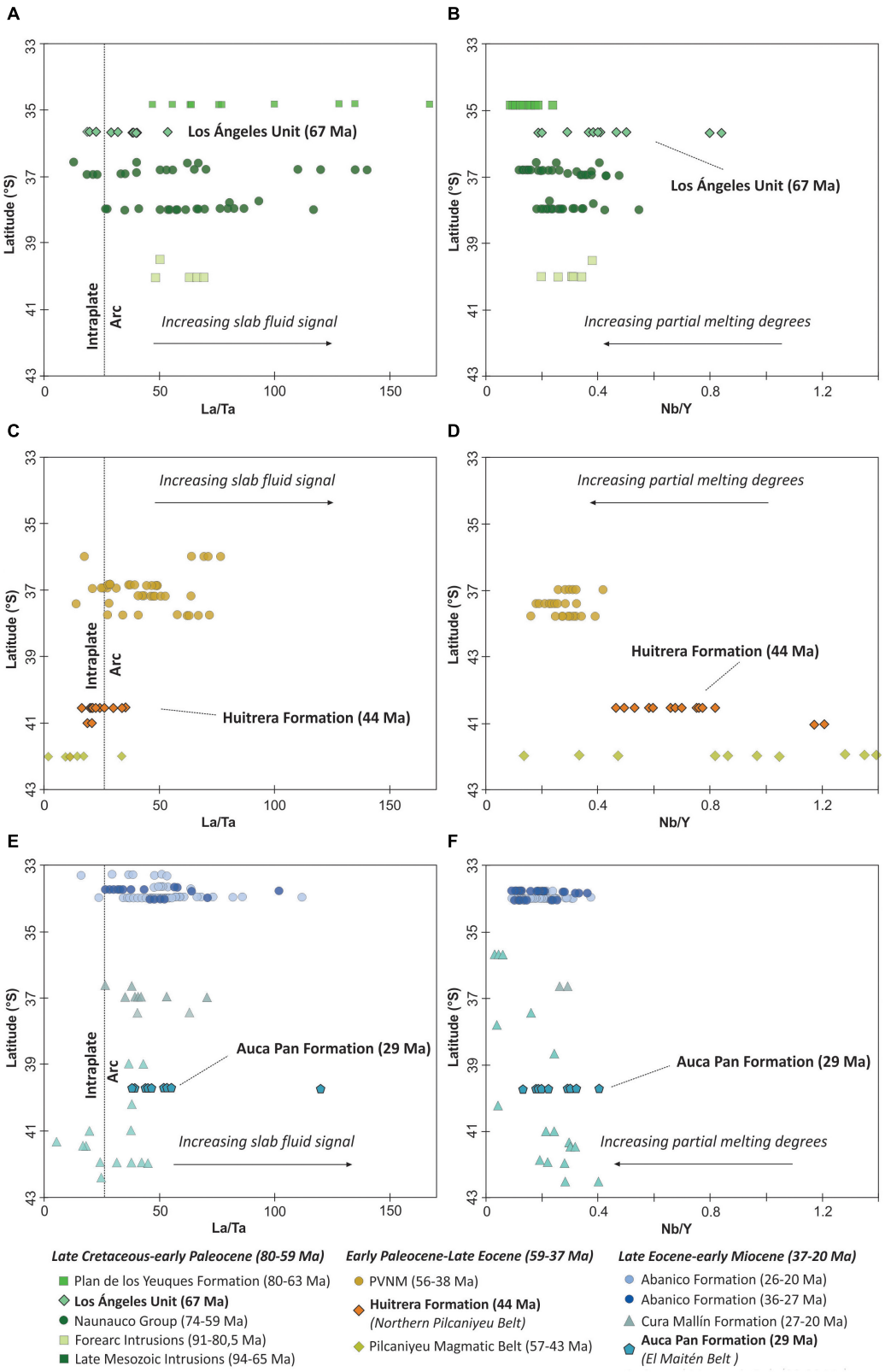

FIGURE 12 | (A,B) Latitude °(S) vs. La/Ta and Latitude (°S) vs. Nb/Y for Late Cretaceous-early Paleocene magmatic units along the Southern Central Andes. **(C,D)** Latitud (°S) vs. La/Ta and Latitude (°S) vs. Nb/Y for early Paleoceno-late Eocene magmatic units along the Southern Central Andes. **(E,F)** Latitud (°S) vs. La/Ta and Latitude (°S) vs. Nb/Y for late Eocene-early Miocene magmatic units along the Southern Central Andes. These diagrams show the variations in slab-fluid influence and partial melting degrees regarding the time and location of emplacement for each magmatic sequence.

between 36° and 41°S. However, a tholeiitic to slightly alkaline and more enriched magmatism is registered at 35°30′S (Los Ángeles Unit), which, together with the presence of adakite-like intrusions at 39°S (De La Fuente, 2014), may indicate variable magmatic sources and/or geochemical process, affecting Andean magmatism during this stage.

Late Paleocene–Middle Eocene Magmatic Evolution

The late Paleocene–middle Eocene magmatic stage (59–37 Ma) is characterized by the development of arc-related sequences with contrasting geochemical signatures and a limited and disperse distribution (**Figures 1**, **6**). Along the Andean margin, between the studied latitudes (35–42°S), a magmatic lull is registered at 34–36°S (**Figure 1**). Southwards (36–38°S), late Paleocene–middle Eocene arc-related magmatism is recognized as the *Provincia Volcánica Neuquino Mendocina* (PVNM) developed from 56 to 38 Ma (Llambías and Rapela, 1989; Kay et al., 2006). Coevally, but in a eastern retroarc position, at 40–43°S, the magmatic products of the Pilcaniyeu Belt (Huitrera Formation) are exposed with a NW–SE direction (57–43 Ma; Rapela et al., 1983, 1988; Aragón et al., 2011, 2018), whose northern outcrops (40°S) correspond to the studied area (44 Ma; Iannelli et al., 2017).

From north to south, arc-like magmatism between 36° and 38°S (PVNM) presents a strong arc-like imprint (**Figures 11C,D**, **12**). In contrast, immediately to the south at 40°S, studied Huitrera Formation (44 Ma; Northern Pilcaniyeu Belt) shows minor arc-like signature given the lower Th/Hf, La/Ta, and the higher Ce/Pb, and a tendency toward an alkaline composition, as shown by higher Ta/Hf, Nb/Yb, and Nb/Y ratios (**Figures 11C,D**, **12**). Furthermore, Eocene Huitrera Formation at 40°S, presents lower Sr isotopic signature for a similar εNd range relative to the northern coeval magmatism (PVNM, 36–38°S) (**Figure 7B**).

When considering the late Paleocene–early Eocene magmatism (Pilcaniyeu Belt; ∼57–43.1 Ma) emplaced at 40–43°S in the Patagonian Precordillera, a decrease in arc-like influence with an increase in alkaline composition are recognized from the northern (40°S) to the southern (42–43°S) outcrops of this belt. This is shown by the higher Ta/Hf and lower Th/Hf, Ce/Pb, and La/Ta ratios seen in the southern outcrops (42–43°S) relative to the northern ones (**Figures 11C,D**, **12A**). The higher Nb/Yb and Nb/Y ratios in the southern sections (42–43°S) also indicate lower melting degrees relative to the northern studied sequence (40°S) (**Figures 11D**, **12B**). This magmatism has been described as the products of extensional collapsed calderas associated with an intraplate setting and the development of a slab window (Aragón et al., 2011, 2013, 2018). The isotopic signature of these southern outcrops (42–43°S) is variable, but showing partially higher εNd and lower $(^{87}Sr/^{86}Sr)_i$ that the studied northern sequences of Huitrera Formation at 40°S (**Figure 7B**; Aragón et al., 2011, 2018).

Late Eocene–Early Miocene Magmatic Evolution

By the last magmatic period (37–20 Ma) Andean arc-like sequences show a more widespread and continuous distribution in comparison with the previous magmatic stages, as well as less pronounced geochemical differences. A regional comparison is made between studied Auca Pan Formation (29 Ma, 39°S; Iannelli et al., 2017), the volcanic units of the Abanico Formation emplaced at 33–36°S (36–20 Ma; Charrier et al., 2002; Kay et al., 2005; Muñoz et al., 2006; Piquer et al., 2017), the lower sections of the Cura Mallín Formation at 36–38°S (27–20 Ma; Suárez and Emparán, 1995; Burns et al., 2006; Kay et al., 2006; Utgé et al., 2009), and the southern Coastal Magmatic Belt developed between 37° and 43.5°S (28–20 Ma; López-Escobar and Vergara, 1997; Muñoz et al., 2000; **Figure 1**).

Between 37 Ma and 25 Ma, arc sequences were recognized at the Southern Central Andes mainly between 33° and 36°S (Abanico Formation), whereas in the North Patagonian Andes, the late Eocene–early Oligocene period comprises studied volcanism from the Auca Pan Formation (29 Ma; 39°S) (**Figure 1**). Both units share a slab-fluid signal and a partially calc-alkaline source as shown by the high Th/Hf and low Ce/Pb, Ta/Hf, and Nb/Yb (**Figures 11E,F**). Changes in geochemical signature are seen after ∼26–23 Ma, when this magmatism developed strongly controlled by the widespread extensional conditions. This younger magmatism developed along the Southern Central Andes between 33° and 38°S (Abanico Formation, ∼26–20 Ma; Cura Mallín Formation, ∼27–20 Ma) and southwards, mainly located in the fore-arc area, between 37° and 43.5°S (Coastal Magmatic Belt; 28–20 Ma) (**Figures 1**, **6**). Overall, magmatism within 26–23 Ma presents a strong tholeiitic signature with partially higher slab-fluid influence and higher melting degrees than 37–25 Ma magmatic sequences (**Figures 7C**, **11E,F**). Decreasing Sr and increasing Nd isotope ratios are seen toward these younger magmatic units, indicating also an increasing influence of a depleted mantle source (**Figure 7C**). A decrease in $^{206}Pb/^{204}Pb$ and similar values of $^{207}Pb/^{204}Pb$ and $^{208}Pb/^{204}Pb$ are seen when comparing the younger magmatism of the Coastal Magmatic Belt (28–20 Ma; 37–43.5°S) with the partially older Auca Pan Formation (29 Ma) (**Figures 7C**, **8E,F**; López-Escobar and Vergara, 1997; Muñoz et al., 2000).

Integrated Tectonic Evolution

During the Late Cretaceous, the Farallon–Aluk spreading ridge began to interact with the Andean margin at ∼30°S (Seton et al., 2012; Müller et al., 2016; Wright et al., 2016). This segmented spreading ridge moved southwards, and by 70 Ma, it was subducting at ∼35°S with an NW- to NNW-directed motion, reducing dramatically the convergence velocity and so leading to plate divergence despite the continued westward motion of the South American plate (Somoza and Ghidella, 2005; Müller et al., 2016; Wright et al., 2016). At this time, the South American upper plate kinematics had no significant role in the upper plate tectonic regime as a reduction in trench normal upper plate motion from ∼2 to ∼1 cm/year is only observed at ∼65 Ma (see **Figure 4**, Maloney et al., 2013) after the onset of extension in several areas (Cornejo et al., 1994; Emparán and Pineda, 1997, 2000; Ladino et al., 2000; Aragón et al., 2011; Muñoz et al., 2018; Fennell et al., 2019). Also, the fact that current values of trench normal absolute motion of the South American plate, lower than those between 65 and 45 Ma (see **Figure 4**; Maloney et al., 2013), cause significant neotectonic contractional activity in Central Andes (see Costa et al., 2006 for a synthesis) precludes linking

extension to upper-plate motion at this time. The negative to closely neutral convergence velocity between 20°S and 36°S (i.e., plate divergence) (Maloney et al., 2013; **Figure 4**), responsible for the widespread deformation, would have been caused by the demise of the obliquely subducting Farallon–Chasca and Chasca–Catequil mid-ocean ridges that were producing a fast and roughly orthogonal subduction of the Chasca plate and onset of subduction of the Farallon–Aluk mid-ocean ridge plate at studied latitudes, causing the Farallon plate and so the Farallon–Aluk spreading ridge to subduct with a NW to NNW direction (Müller et al., 2016; Wright et al., 2016). This process reduced dramatically the convergence velocity leading to plate divergence despite the continued westward motion of South America to the west (Müller et al., 2016; Wright et al., 2016).

Meanwhile, Late Cretaceous–early Paleocene arc-related magmatism shows a scattered occurrence with significant magmatic gaps along the Southern Central Andes (**Figures 1**, **13A**). Contrasting geochemical signatures from typical arc-like to more enriched geochemical compositions are seen between the magmatic units considered in this work. Los Ángeles Unit magmatism (35°30′S; 67 Ma) presents a transitional alkaline-like signature and an OIB-like isotopic composition emplaced in an extensional setting, however, immediately to the north (Plan de los Yeuques Formation; 34°30′S) and to the south (Naunauco Group, 36–38°S; Late Cretaceous intrusives, 36°–41°S), magmatic activity shows a typical arc-like geochemical behavior and variable depleted isotopic compositions (**Figures 7A**, **11**) (see discussion in section Late Cretaceous-Early Paleocene Magmatic Evolution). Furthermore, by the same time, adakite-like intrusions also appeared in the fore-arc zone at ∼39°S (De La Fuente et al., 2012, De La Fuente, 2014).

In addition, coeval synextensional magmatism emplaced in arc to back-arc settings with alkaline and enriched signatures is also described northwards of the studied region (**Figure 13A**), as the alkaline lavas and dikes from the Cerro Totola Formation (66 Ma, 22–24°S, Mpodozis et al., 2005), the back-arc enriched basalts of the Río Frío Formation (∼56 Ma, 29°50′S) (Litvak et al., 2007; Jones et al., 2016), and the rift sequences depicted at 32°S by Lucassen et al. (2002). Coeval extensional settings are also described between the Coquimbo (30°S), El Salvador (26°S), and Calama (23°S) areas, where Late Cretaceous–early Paleocene (∼85–65 Ma) collapse magmatic calderas have been described, associated with extensional settings and indicating a change between arc-like to intraplate magmatic products (**Figure 13A**; Rivera and Mpodozis, 1991, 1994; Arévalo et al., 1994; Cornejo et al., 1994; Emparán and Pineda, 1997, 2000; Cornejo and Mathews, 2000; Ladino et al., 2000). Most of these latest Cretaceous–early Paleocene sequences have been associated with the highly oblique subduction of the Farallon plate during this studied period (Cornejo et al., 1994; Emparán and Pineda, 1997, 2000; Cornejo and Mathews, 2000).

On the other hand, the joint analysis of P- and S-seismic tomography and plate kinematic reconstructions supports the existence of a slab gap below the study area during the Late Cretaceous times (**Figures 9**, **10A**), which is interpreted as a relict of the Late Cretaceous slab window that is still preserved in the uppermost lower mantle. This behavior can be comparable with an analog model documented in western North America and eastern Sumatra (Fabian et al., 2010; Gaina and Jakob, 2019). The location of the enriched sequences emplaced in extensional settings is consistent with the areas affected by the collision of the Farallon–Aluk spreading ridge according to the tomography results (**Figure 13A**). Thus, the contrasting geochemical signature between neighboring coeval units, the presence of adakite-like intrusions in the fore-arc, and the extensional regimen recognized in the overriding plate, could be related to the initial passage of the segmented Farallon–Aluk spreading ridge and the beginning of its influence in the Andean magmatism at the studied latitudes (35–42°S) (**Figure 15A**; Iannelli et al., 2018). The oblique collision of a segmented spreading ridge as the Farallon–Aluk would have probably favored the development of diachronic slab windows or at least the participation of more enriched mantle sources that affected discrete portions of the Andes since Late Cretaceous times (Thorkelson, 1996; Somoza and Ghidella, 2005). The contrasting angle and direction of subduction between both plates during their southward migration controlled the full development of the slab windows with time (Thorkelson, 1996; Somoza and Ghidella, 2005, 2012). In consequence, the subduction and simultaneous migration of this segmented spreading ridge could explain the emplacement of the contrasting but coeval magmatic units along the Andean margin, and the participation of an enriched and isotopically depleted mantle source for studied Los Ángeles magmatism during this period (**Figures 13A**, **14A**).

Modern analogs have also been used to finally interpret the Los Ángeles Unit volcanism and justify this premise, as for example the Neogene Plateau lavas in Patagonia (46.5–49.5°S) (Gorring and Kay, 2001; Guivel et al., 2006) associated with the collision of the Chilean Ridge. The similar isotopic signature, partially similar geochemical composition (**Figures 5**, **7A**, **11**), and the tectonic context between the Neogene plateau lavas and the Los Ángeles Unit could be in favor of a similar magmatic origin for the evolution of both sequences. In particular, Los Ángeles Unit shows an arc-like signature partially higher than the plateau lavas (**Figures 11A,B**), which can be explained due to their position closer to the Andean arc. The origin of the Neogene Plateau lavas has been attributed to the melting of limited OIB-like heterogeneities in a depleted MORB-like subslab asthenosphere (Gorring and Kay, 2001; Gorring et al., 2003). In this case, the mixing with "stored" arc components at the base of the continental lithosphere was also considered (Gorring and Kay, 2001; Espinoza et al., 2005). Furthermore, the tholeiitic composition register in the initial levels of Los Ángeles Unit magmatism is consistent with the ascent and decompression melting of hot asthenospheric mantle associated to the opening of a slab window, as proposed for the Eocene magmatism during the Caribbean–North America–Farallon triple boundary evolution in Mexico (e.g., Ferrari et al., 2014).

For the early Paleocene–late Eocene period (∼59–37 Ma), the combined analysis of seismic tomography and plate kinematic reconstruction indicates that the previous slab gap migrated southwards following the kinematics of the Farallon–Aluk–South American triple junction (**Figures 10B**, **13B**). During this period,

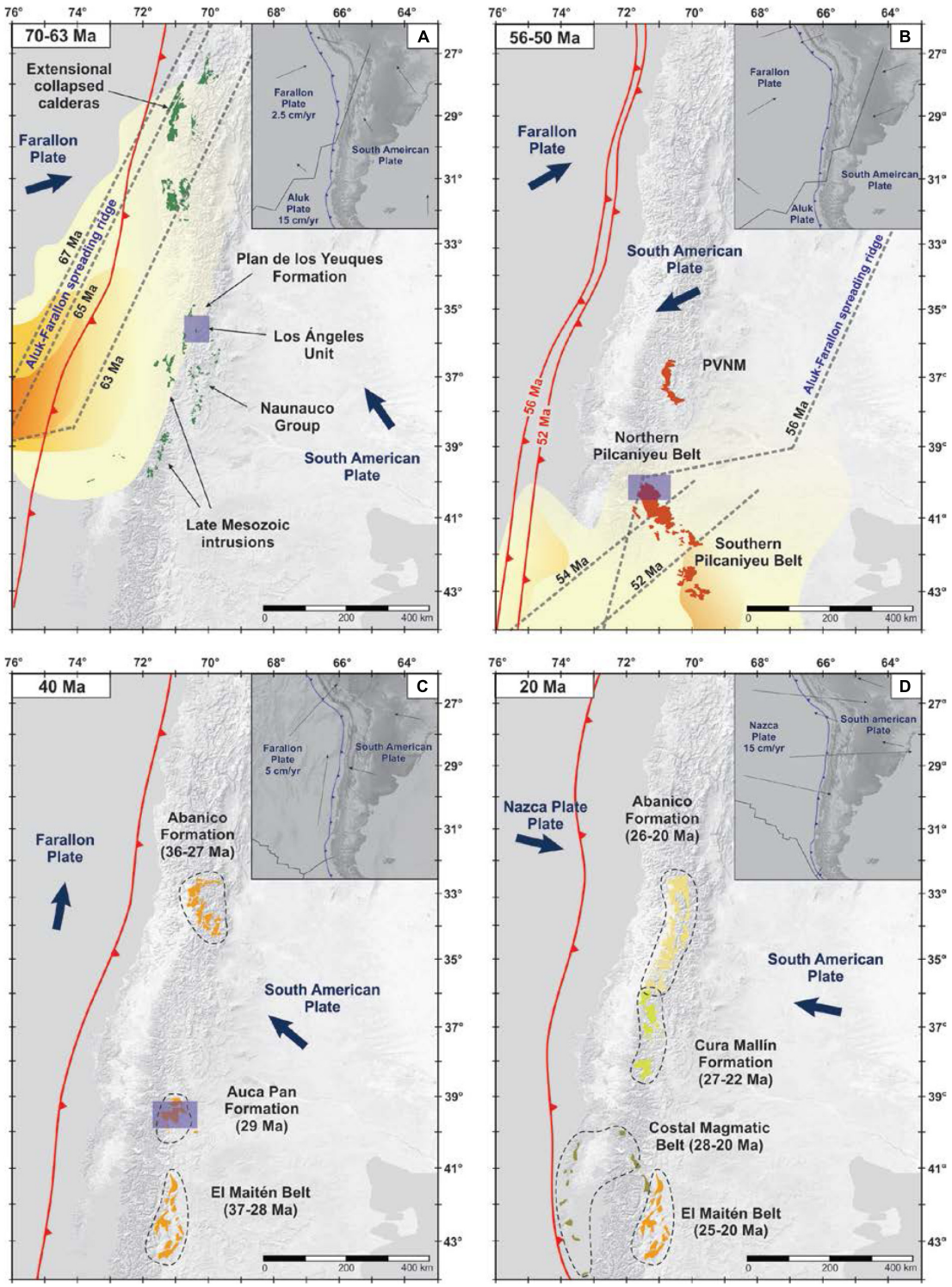

FIGURE 13 | (A,B) Schematic maps that represent the southward movement of the Farallon–Aluk spreading ridge for the Late Cretaceous–early Paleocene (70–63 Ma) and the early Eocene (56–50 Ma) period. The orange to yellow field represents the location of the Farallon–Aluk spreading ridge according to the tomography results. The blue shaded squares show the studied areas in each figure. The green outcrops represented in **(A)** corresponds to the Late Cretaceous–early Paleocene magmatism (80–59 Ma) while the orange outcrops in **(B)** are the early Paleocene–late Eocene magmatism (59–37 Ma). **(C)** Late Eocene–early Oligocene magmatic units emplaced along the Southern Central Andes (35–42°S). Blue arrows represent the convergence direction for both the Farallon and South American plates. **(D)** Early Oligocene–early Miocene magmatic units emplaced along the Southern Central Andes after Farallon plate break-up. In this case, blue arrows represent the convergence direction for both Nazca and South American plates.

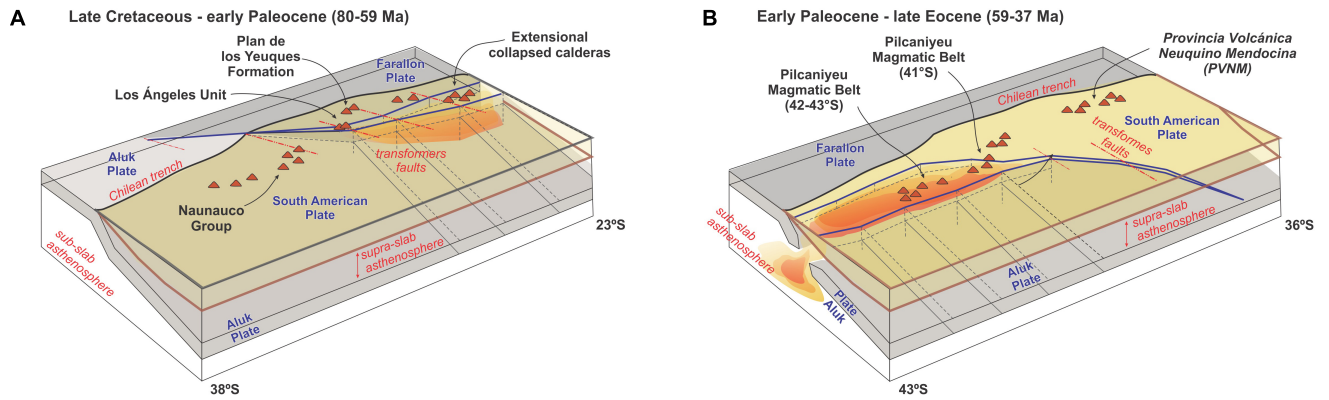

FIGURE 14 | Schematic model representing the passage of the Farallon–Aluk spreading ridge since **(A)** Late Cretaceous–early Paleocene time (80–59 Ma) to **(B)** Early Paleocene–late Eocene (59–37 Ma), and the main magmatic units from each period.

the Farallon–Aluk spreading ridge reached Patagonian latitudes (Espinoza et al., 2005; Breitsprecher and Thorkelson, 2009), while northwards the Farallon plate was subducting with a NE direction beneath the South American plate (Somoza and Ghidella, 2012). The high degrees of obliquity partially decrease by 49 Ma, but remained during most of this stage, triggering an extensional regime in the upper plate (Pardo-Casas and Molnar, 1987; Somoza and Ghidella, 2005; Müller et al., 2016).

Magmatism during this period (59–37 Ma) is also characterized by the emplacement of coeval magmatic units with contrasting geochemical signatures as in the former magmatic period (80–59 Ma) (**Figure 13B**). In this sense, Eocene magmatism at 36–38°S (PVNM) presents a geochemical and isotopic composition typical of an arc-like magmatism with a calc-alkaline source that differs from the transitional to intraplate-like character seen along the Paleocene–early Eocene magmatism between 40° and 43°S (Pilcaniyeu Belt–Huitrera Formation) (**Figures 11B,C**, **12A,B**, **13B**). This southern magmatic unit (57–43 Ma) developed in a retroarc position with a NW–SE direction between 40° and 43°S (**Figure 13B**). Geochemical differences have been distinguished along this magmatic belt. Toward the north (40°S), the studied magmatic sequences (northern Pilcaniyeu Belt, Huitrera Formation; 44 Ma) (**Figure 15B**) show a transitional subalkaline to alkaline signature with minor slab-fluid influence (**Figures 4A**, **11B,C**, **12A,B**). In contrast, southern magmatic collapse calderas at 42–43°S (∼57–43 Ma) show a pronounced intraplate character, which have been associated with the development of a slab window based on their geochemical signatures and a 2-D seismic tomography cross-section showing a detached slab in the mantle transition zone (**Figures 13B**, **14B**; Aragón et al., 2011, 2013). The increment of an arc-like signature in the northern and also younger outcrops of this magmatic belt (Huitrera Formation; 44 Ma; 40°S) is consistent with its position closer to the arc-zone and its development during the last influences of the subducting spreading ridge (Iannelli et al., 2017; **Figures 13B**, **14B**).

Hence, the new isotopic data from Eocene magmatism at 40°S, and its regional comparison with coeval units, together with horizontal seismic tomography slice data presented in this study, allow confirming the existence of this slab gap and unraveling the regional extent of this tectonic feature (**Figures 10B**, **13B**, **14B**). The segmented magmatic and tectonic nature of Patagonia during this period have already been associated with the development of a slab-window event (e.g., Ramos and Kay, 1992; Espinoza et al., 2005) and more recently with diachronic slab windows (Gianni et al., 2018b). Thus, the presence of the active spreading ridge in Patagonian latitudes can explain the geochemically contrasting magmatic sequences and the gaps between them (**Figures 10B**, **13B**, **14B**).

Previous plate kinematic reconstructions suggested that after the final subduction of the Aluk plate at ∼40–35 Ma, Farallon plate was subducting with a highly oblique direction and low convergence rate beneath the South American plate (Cande and Leslie, 1986; Somoza and Ghidella, 2005). By late Oligocene times, Farallon plate finally broke up into Nazca and Cocos plates, and consequently, Nazca plate started to subduct with an orthogonal direction and high-velocity rates (∼15 cm/year) (Pardo-Casas and Molnar, 1987; Somoza and Ghidella, 2012). The combined analysis of seismic tomography and plate kinematic reconstruction indicates that, at that time, the slab gap positioned below the southern sector of South America and the fast anomaly linked to the presence of the subducted slab propagated southward, forming a continued subduction zone (**Figures 10C**, **13C,D**).

As recently suggested by the numerical modeling presented in Fennell et al. (2018), this new subduction zone triggered extensional conditions along the Southern Central and Patagonian Andean margin as the tip of the slab subducted rapidly before approaching the mantle transition zone (e.g., Jordan et al., 2001; Fennell et al., 2018). The new tectonic conditions affected directly the development of the late Eocene–early Miocene magmatism, which presents variable geochemical signatures with time along the North Patagonian Andes (**Figure 13C**).

Late Eocene–early Oligocene volcanism is recognized with an N–S distribution all along the Southern Central and North

Patagonian Andes between 33° and 43°S (Abanico Formation, Auca Pan Formation and the El Maitén Belt). In the studied area (39 Ma), Auca Pan Formation (29 Ma) shows an arc-like calc-alkaline composition with an isotopic signature that resembles an arc-like source. Coeval magmatism in the Andean margin is also recognized northwards between 33° and 36°S, in the oldest magmatic pulses of the Abanico Formation (∼36–27 Ma), which present a partially similar geochemical character to the Auca Pan Formation (29 Ma). To the south, arc resumption was characterized by an initially arc-like tholeiitic composition that progressively shows a more calc-alkaline signature (Fernández Paz et al., 2018, 2019).

After the major tectonic changes by latest Oligocene (∼25–23 Ma), extensional conditions fully installed in the Andean margin, leading to the expansion of a widespread magmatism and the southern thinning of the continental crust. The new tectonic parameters of the newly Nazca plate provoked a period of roll-back that affected the Oligocene–early Miocene sequences (**Figure 13C**; Muñoz et al., 2000; Jordan et al., 2001). These tectonic changes are consistent with the involvement of a more depleted mantle source and the rapid emplacement of this tholeiitic magmatism without interaction with the continental crust (e.g., Muñoz et al., 2000). In consequence, the lower Cura Mallín Formation (27–20 Ma; 36–38°S) (Suárez and Emparán, 1995; Jordan et al., 2001) and the upper magmatic levels of the Abanico Formation (∼26–20 Ma; 33–36°S) (Charrier et al., 2002; Kay et al., 2005; Muñoz et al., 2006) show a tholeiitic imprint and an isotopic composition typical of a depleted mantle source (**Figures 7C**, **11E,F**, **13C**). North Patagonian volcanism at 40–43°S shows again a tholeiitic and depleted imprint (Litvak et al., 2014; Fernández Paz et al., 2018, 2019), partially similar to the arc-like tholeiitic and isotopically depleted coeval magmatism emplaced in the Central Depression between 37° and 43.5°S (**Figure 13C**) (Coastal Magmatic Belt; 28–20 Ma) (López-Escobar and Vergara, 1997; Muñoz et al., 2000).

CONCLUSION

Early Cenozoic magmatic arc had experienced compositional and geodynamic changes in response to the interaction of a spreading ridge with the South American margin between 35 and 42°. Based on the three independent methodologies—(i) Sr, Nd, and Pb isotopic analysis; (ii) seismic tomography; and (iii) kinematic reconstructions – we provided evidence of the extent and the consequences in arc magmatism of the migration of the Farallon–Aluk ridge from the Late Cretaceous to middle Eocene. Thus, along the Andean magmatic arc, some areas show isotopic compositions that reflect partially enriched mantle sources: the Los Ángeles Unit (69 Ma; 35°30′S) and the Huitrera Formation (44 Ma; 40°S). On the other hand, the tomotectonic analysis, together with the kinematic reconstructions, revealed a slab gap that correlates with the occurrence of these enriched portions of the asthenospheric wedge. Our model shows the interaction of the Farallon–Aluk spreading ridge with the South American margin, whereas, integrated in a regional magmatic context, it provides robust evidence about the existence of a slab window event by latest Cretaceous–early Paleocene times and its southward migration along the Southern Central Andes till Eocene times.

In the Southern Central Andes (∼35°S), the interaction of the Farallon–Aluk mid-ocean ridge with the Andean margin would have promoted extensional deformation during Latest Cretaceous–early Paleocene times (80–59 Ma), the development of the collapse calderas magmatism in the north (23–28°S), the transitional intraplate-like magmatic character recognized in specific arc-related magmas (35°30′S), and the presence of adakite-like intrusions in the fore-arc area (39°S). Despite the fact that the influence of this spreading ridge would have better developed in the north (∼23–28°S), the Los Ángeles Unit (35°30′S) reflects a trend from tholeiitic to a more alkaline enriched composition with isotopically depleted mantle sources. Meanwhile, to the south of the Los Ángeles Unit, a typical arc developed without influence of this spreading ridge (∼36–38°S). The contrasting geochemical composition between coeval magmatism during the Late Cretaceous–early Paleocene is consistent with the segmented configuration of the Farallon–Aluk spreading ridge. In the North Patagonian Andes (39–43°S), the segmented distribution and composition seen in early Paleocene–late Eocene magmatism (59–37 Ma) similar to the previous period (80–59 Ma) is also consistent with the tomography sections that tracked the location of the triple junction point toward the south. By this period, the Farallon–Aluk spreading ridge moved toward Patagonian latitudes where an asthenospheric window developed (42–43°S) and caused the emplacement of intraplate-like magmatism. In contrast, northern coeval sequences (36–38°S) showed a typical arc-like signature. The geochemical composition of coeval magmatism fully coincides with tomography sections that show an anomaly at 42°S, while northwards, a normal subduction setting was developing.

Finally, by the late Eocene–early Miocene period, a typical arc-like magmatism developed, consistent with the establishment of a continuous subduction zone as seen in the tomography sections. New isotopic data show the participation of arc-like sources with minor crustal contribution, consistent with the development of the calc-alkaline arc magmatism of the Auca Pan Formation (29 Ma). A more depleted mantle source is seen for the late Oligocene–early Miocene related to the major tectonic reconfiguration at 25–23 Ma.

DATA AVAILABILITY STATEMENT

All datasets generated for this study are included in the article/**Supplementary Material**.

AUTHOR CONTRIBUTIONS

SI, LF, and VL are specialists in the interpretation and use of geochemical data and experts in petrogeneis of magmatic suites. GG contributed to tomography reconstructions and modeling while LF and AF contributed to structural field data and tectonic interpretation. JG and VO helped with the lab work and

isotopic data. FL and SK made it possible to obtain the complete amount of isotopic data in the Geochemical Lab of the MARUM Institute at the University of Bremen (Germany) and helped to improve the isotopes interpretation.

ACKNOWLEDGMENTS

We specially acknowledge the two reviewers and the editor Dr. Marina Manea for their fruitful suggestions that improved this manuscript. We also acknowledge the financial support from CONICET (grant 11220150100426CO), University of Buenos Aires (grant UBACYT 20020150100166BA), and ANPCyT (PICT-2012-1490 and PICT-2014-2240).

SUPPLEMENTARY MATERIAL

The Supplementary Material for this article can be found online at: https://www.frontiersin.org/articles/10.3389/feart.2020.00121/full#supplementary-material

REFERENCES

Aguirre Urreta, B., Tunik, M., Naipauer, M., Pazos, P., Ottone, E., Fanning, M., et al. (2011). Malargüe Group (Maastrichtian-Danian) deposits in the neuquén andes, argentina: implications for the onset of the first atlantic transgression related to western gondwana break-up. *Gond. Res.* 19, 482–494. doi: 10.1016/j.gr.2010.06.008

Amaru, M. (2007). *Global Travel Time Tomography with 3-D Reference Models, Geology Traiectina*. Ph. D. thesis, University of Utrecht, Utrecht.

Aragón, E., Castro, A., Díaz-Alvarado, J., Pinotti, L., Fernando, D., Demartis, M., et al. (2018). Mantle derived crystal-poor rhyolitic ignimbrites: eruptive mechanism from geochemical and geochronological data of the Piedra Parada caldera, Southern Argentina. *Geosci. Front.* 9, 1529–1553. doi: 10.1016/j.gsf.2017.09.004

Aragón, E., D'Eramo, F., Castro, A., Pinotti, L., Brunelli, D., Rabbia, O., et al. (2011). Tectono-magmatic response to major convergence changes in the North Patagonian suprasubduction system; the Paleogene subduction–transcurrent plate margin transition. *Tectonophysics* 509, 218–237. doi: 10.1016/j.tecto.2011.06.012

Aragón, E., Pinotti, L., D'Eramo, F., Castro, A., Rabbia, O., Coniglio, J., et al. (2013). The farallon-aluk ridge collision with south america: implications for the geochemical changes of slab window magmas from fore- to back-arc. *Geosci. Front.* 4, 377–388. doi: 10.1016/j.gsf.2012.12.004

Arévalo, C., Rivera, O., Iriarte, S., and Mpodoszis, C. (1994). Cuencas extensional y campos de calderas del Cretácico Superior-Terciario inferior en la precordillera de Copiapó (27°-28°S), Chile in VII Congreso Geológico Chileno Concepción. *J. Geophys. Res.* 2, 1288–1292.

Ávila, P., and Dávila, F. M. (2018). Heat flow and lithospheric thickness analysis in the Patagonian asthenospheric windows, southern South America. *Tectonophysics* 747, 99–107.

Basei, M., Ramos, V. A., Vujovich, G. I., and Poma, S. (1999). El basamento metamórfico de la Precordillera Frontal de Mendoza: nuevos datos geocronlógicos e isotópicos" in X Congreso Latinoamericano de Geología y VI congreso nacional de geología económica actas. *J. Geophys. Res.* 2, 412–417.

Bechis, F., Encinas, A., Concheyro, A., Litvak, V. D., Aguirre-Urreta, B., and Ramos, V. A. (2014). New age constraints for the Cenozoic marine transgressions of northwestern Patagonia, Argentina (41–43°S): paleogeographic and tectonic implications. *J. S. Am. Earth Sci.* 52, 72–93.

Billen, M. I. (2008). Modeling the dynamics of subducting slabs. *Annu. Rev. Earth Planet. Sci.* 36, 325–356.

Braz, C., Seton, M., Flament, N., and Müller, R. D. (2018). Geodynamic reconstruction of an accreted Cretaceous back-arc basin in the Northern Andes. *J. Geodyn.* 121, 115–132.

Breitsprecher, K., and Thorkelson, D. J. (2009). Neogene kinematic history of Nazca–Antarctic–Phoenix slab windows beneath Patagonia and the Antarctic Peninsula. *Tectonophysics* 464, 10–20.

Burns, W. M., Jordan, T. E., Copeland, P., and Kelley, S. A. (2006). "The case for extensional tectonics in the Oligocene-Miocene Southern Andes as recorded in the Cura Mallín basin (36°–38°S)," in *Evolution of an Andean Margin: A Tectonic And Magmatic View From The Andes To The Neuquén Basin (35°–39°S lat)*, Vol. 407, eds S. M. Kay and V. A. Ramos (Boulder: Geological Society of America), 163–184. doi: 10.1130/2006.2407(08)

Cande, S. C., and Leslie, R. B. (1986). Late cenozoic tectonic of the Southern Chile Trench. *J. Geophys. Res.* 91, 471–496.

Casé, A. M., López-Escobar, L., Danieli, J. C., and Schalamuk, A. (2008). Butalón igneous rocks, Neuquén, Argentina: age, stratigraphic relationships and geochemical features. *J. S. Am. Earth Sci.* 26, 188–203.

Cazau, L., Mancini, D., Cangini, J., and Spalletti, L. (1989). "Cuenca de Nirihuau," in *Cuencas Sedimentarias Argentinas*, Vol. 6, eds G. Chebli and L. Sapalletti (London: Serie Correlación Geológica), 299–318.

Charrier, R., Baeza, O., Elgueta, S., Flynn, J., Gans, P., Kay, S. M., et al. (2002). Evidence for Cenozoic extensional basin development and tectonic inversion south of the flat-slab segment, southern Central Andes Chile, (33°–36°S). *J. S. Am. Earth Sci.* 15, 117–139.

Charrier, R., Pinto, L., and Rodríguez, M. P. (2007). "Tectonostratigraphic evolution of the Andean Orogen in Chile," in *The Geology of Chile*, eds T. Morenoand and W. Gibbons (London: Geology Society), 21–114.

Charrier, R., Wyss, A., Flynn, J. J., Swisher, C. C., Norell, M. A., Zapatta, F., et al. (1996). New evidence for late Mesozoic-early Cenozoic evolution of the Chilean andes in the upper tinguiririca valley (35°S), central Chile. *J. South Am. Earth Sci.* 9, 393–422. doi: 10.1016/S0895-9811(96)00035-1

Chen, Y. W., Wu, J., and Suppe, J. (2019). Southward propagation of Nazca subduction along the Andes. *Nature* 565, 441–447. doi: 10.1038/s41586-018-0860-1

Cornejo, P., and Mathews, S. (2000). "Relación entre magmatismo-tectónica y su implicancia en la formación de sistemas de pórfiros cupríferos: yacimiento El Salvador, 3 Región, Chile," in *Proceedings of the IX Congreso Geológico Chileno*, Puerto Varas.

Cornejo, P. C., Mpodozis, C., Kay, S. M., and Tomlianson, A. J. (1994). "Volcanismo Bimodal Potásico en Regimen Extensional del Cretácico Superior-Eoceno en la región de El Salvador (26-27°),"in *Proceedings of the VII Congreso Geológico Chileno Concepción, Actas*, Chile.

Dalla Salla, L., Leguizawjn, M., Mazzoni, M., Merodlo, J., Rapela, C., and Spalletti, L. (1981). *Características del vulcanismo paleógeno en la Cordillera Nordpatagónica entre las latitudes 39°30' y 41°20' S", in VIII Congreso Geológico Argentino*. Chile: University of Concepcion.

De La Fuente, D., Figueroa, O., Duhart, P., Quiroz, D., Demaiffe, D., Oliveros, V., et al. (2012). *Los* intrusivos de Antearco del Cretácico Superior de Chile Centro Sur (39°S-40°S): Petrografía y geoquímica," in *XIII Congreso Geológico Chileno Actas*. 336–338.

De La Fuente, D. A. (2014). *Los Intrusivos de Ante-Arco Del Cretácico Su'Perior Del Centro-Sur De Chile (39-40°S): Petrografía y Geoquímica*. Master thesis, University of Concepción, Chile.

DeLong, S. E., Schwarz, W. M., and Anderson, R. N. (1979). Thermal effects of ridge subduction. *Earth Planet. Sci. Lett.* 44, 239–246.

Deruelle, B. (1982). Petrology of the Plio-Quaternary volcanism of the south-central and meridional Andes. *J. Volcanol. Geotherm. Res.* 14, 77–124.

Dickinson, W. R., and Snyder, W. S. (1979). Geometry of triple junctions related to San Andreas transform. *J. Geophys. Res.* 84, 561–572.

Domeier, M., Doubrovine, P. V., Torsvik, T. H., Spakman, W., and Bull, A. L. (2016). Global correlation of lower mantle structure and past subduction. *Geophys. Res. Lett.* 43, 4945–4953. doi: 10.1002/2016GL068827

D'Orazio, M., Agostini, S., Mazzarini, F., Innocenti, F., Manetti, P., Haller, M. J., et al. (2000). The Pali Aike Volcanic Field, Patagonia: slab-window magmatism near the tip of South America. *Tectonophysics* 321, 407–427.

Eagles, G., and Scott, B. G. (2014). Plate convergence west of Patagonia and the Antarctic Peninsula since 61 Ma. *Glob. Planet. Chang.* 123, 189–198.

Emparán, C., and Pineda, G. (2000). Estratigrafía y geocronología U-Pb y K-Ar de los sistemas volcánicos del Cretácico superior- Paleógeno en la zona de Condoriaco-Rivadavia, región de Coquimbo" in IX Congreso Geológico Chileno. *Puerto Varas* 1, 782–786.

Emparán, C. C., and Pineda, G. F. (1997). "El sistema de calderas anidadas Condoriaco (Cretácico superior-Eoceno inferior), IV región de Coquimbo," in *Proceedings of the VIII Congreso Geológico Chileno*, Antofagasta.

Espinoza, F., Morata, D., Pelleter, E., Maury, R. C., Suárez, M., Lagabrielle, Y., et al. (2005). Petrogenesis of the Eocene and Mio–Pliocene alkaline basaltic magmatism in Meseta Chile Chico, southern Patagonia, Chile: Evidence for the participation of two slab windows. *Lithos* 82, 315–343.

Fabian, T., Whittaker, J., and Müller, D. (2010). Mapping Tertiary mid-ocean ridge subduction and slab window formation beneath Sundaland using seismic tomography. *ASEG Extended Abstr.* 1, 1–4.

Fennell, L. M., Iannelli, S. B., Encinas, A., Naipauer, M., Valencia, V., and Folguera, A. (2019). Alternating contraction and extension in the Southern Central Andes (35°–37° S). *Am. J. Sci.* 5, 381–429. doi: 10.2475/05.2019.02

Fennell, L. M., Quinteros, J., Iannelli, S. B., Litvak, V. D., and Folguera, A. (2018). The role of the slab pull force in the late Oligocene to early Miocene extension in the Southern Central Andes (27°-46° S): Insights from numerical modeling. *J. South Am. Earth Sci.* 87, 174–187. doi: 10.1016/j.jsames.2017.12.012

Ferguson, K. M., Dungan, M. A., Davidson, J. P., and Colucci, M. T. (1992). The tatara–san pedro volcano, 36°s, chile: a chemically variable, dominantly mafic magmatic system. *J. Petrol.* 33, 1–43. doi: 10.1093/petrology/33.1.1

Fernández Paz, L., Bechis, F., Litvak, V. D., Echaurren, A., Encinas, A., et al. (2019). Constraints on trenchward arc migration and back-arc magmatism in the North Patagonian Andes in the context of Nazca plate rollback. *Tectonics* 38, 3794–3817. doi: 10.1029/2019TC005580

Fernández Paz, L., Litvak, V. D., Echaurren, A., Iannelli, S. B., Encinas, A., Folguera, A., et al. (2018). Late Eocene volcanism in North Patagonia (42° 30'–43° S): Arc resumption after a stage of within-plate magmatism. *J. Geod.* 113, 13–31. doi: 10.1016/j.jog.2017.11.005

Ferrari, L., Bergomi, M., Martini, M., Tunesi, A., Orozco-Esquivel, T., and López-Martínez, M. (2014). Late Cretaceous-Oligocene magmatic record in southern Mexico: the case for a temporal slab window along the evolving Caribbean-North America-Farallon triple boundary. *Tectonics* 33, 1738–1765.

Folguera, A., Naranjo, J. A., Orihashi, Y., Sumino, H., Nagao, K., Polanco, E., et al. (2009). Retroarc volcanism in the northern San Rafael Block (34°–35°30'S), southern Central Andes: occurrence, age, and tectonic setting. *J. Volcanol. Geotherm. Res.* 186, 169–185.

Folguera, A., and Ramos, V. A. (2011). Repeated eastward shifts of arc magmatism in the Southern Andes: a revision to the long-term pattern of Andean uplift and magmatism. *J. S. Am. Earth Sci.* 32, 531–546.

Folguera, A., Vera, E. R., Bottesi, G., Valcarce, G. Z., and Ramos, V. A. (2010). The Loncopué Trough: a Cenozoic basin produced by extension in the southern Central Andes. *J. Geodyn.* 49, 287–295. doi: 10.1016/j.jog.2010.01.009

Franchini, M. B., Lopez Escobar, L., Shalamuk, I. B. A., and Melnert, L. D. (2003). Paleocene, calc-alkaline subvolcanic rocks from Nevazón Hill area (NW Chos Malal Fold Belt), Neuquén, Argentina, and comparison with granitoids of the Neuqu6n-Mendoza volcanic province. *J. S. Am. Earth Sci.* 16, 399–422.

Futa, K., and Stern, C. R. (1988). Sr and Nd isotopic and trace element compositions of Quaternary volcanic centers of the Southern Andes. *Earth Planet Sci. Lett.* 88, 253–262.

Gaina, C., and Jakob, J. (2019). Global Eocene tectonic unrest: possible causes and effects around the North American plate. *Tectonophysics* 760, 136–151.

Giacosa, R., and Heredia, N. (2001). *Hoja geológica 4172-IV San Carlos de Bariloche*. Buenos Aires: Instituto de Geología y Recursos Minerales.

Giambiagi, L., Mescua, J., Bechis, F., Tassara, A., and Hoke, G. (2012). Thrust belts of the southern Central Andes: along-strike variations in shortening, topography, crustal geometry, and denudation. *Bulletin* 124, 1339–1351. doi: 10.1130/B30609.1

Gianni, G. M., García, H. P., Lupari, M., Pesce, A., and Folguera, A. (2017). Plume overriding triggers shallow subduction and orogeny in the southern Central Andes. *Gondwana Res.* 49, 387–395.

Gianni, G. M., Navarrete, C., and Spagnotto, S. (2019). Surface and mantle records reveal an ancient slab tear beneath Gondwana. *Sci. Rep.* 9:19774. doi: 10.1038/s41598-019-56335-9

Gianni, G. M., Dávila, F. M., Echaurren, A., Fennell, L., Tobal, J., Navarrete, C., et al. (2018a). A geodynamic model linking Cretaceous orogeny, arc migration, foreland dynamic subsidence and marine ingression in southern South America. *Earth Sci. Rev.* 185, 437–462.

Gianni, G. M., Pesce, A., and Soler, S. R. (2018b). Transient plate contraction between two simultaneous slab windows: insights from Paleogene tectonics of the Patagonian Andes. *J. Geody.* 121, 64–75. doi: 10.1016/j.jog.2018.07.008

González Bonorino, F. (1979). Esquema de la evolución geológica de la Cordillera Norpatagónica. *Rev. Asoc. Geol. Argent.* 34, 184–202.

González Bonorino, F., and González Bonorino, G. (1978). Geología de la región de San Carlos de Bariloche. *Rev. Asoc. Geol. Argent.* 33, 175–210.

González Díaz, E. F., and Lizuaín, A. (1984). El Complejo volcano-clástico y plutónico del sector cordillerano. *Geol. Recur. Natur. Río Negro.* 1, 119–129.

Gorring, M., Singer, B., Gowers, J., and Kay, S. M. (2003). Plio–Pleistocene basalts from the meseta del lago buenos aires, argentina: evidence for asthenosphere–lithosphere interactions during slab window magmatism. *Chem. Geol.* 193, 215–235. doi: 10.1016/S0009-2541(02)00249-8

Gorring, M. L., and Kay, S. M. (2001). Mantle processes and sources of Neogene slab window magmas from southern Patagonia, Argentina. *J. Petrol.* 42, 1067–1094. doi: 10.1093/petrology/42.6.1067

Gorring, M. L., Kay, S. M., Zeitler, P. K., Ramos, V. A., Rubiolo, D., Fernandez, M. I., et al. (1997). Neogene Patagonian plateau lavas: continental magmas associated with ridge collision at the Chile triple junction. *Tectonics* 16, 1–17. doi: 10.1029/96TC03368

Groome, W. G., and Thorkelson, D. J. (2009). The three-dimensional thermo-mechanical signature of ridge subduction and slab window migration. *Tectonophysics* 464, 70–83. doi: 10.1016/j.tecto.2008.07.003

Guillaume, B., Martinod, J., Husson, L., Roddaz, M., and Riquelme, R. (2009). Neogene uplift of central eastern Patagonia: dynamic response to active spreading ridge subduction? *Tectonics* 28:TC2009.

Guillaume, B., Moroni, M., Funiciello, F., Martinod, J., and Faccenna, C. (2010). Mantle flow and dynamic topography associated with slab window opening: insights from laboratory models. *Tectonophysics* 496, 83–98.

Guivel, C., Morata, D., Pelleter, E., Espinoza, F., Maury, R. C., Lagabrielle, Y., et al. (2006). Miocene to Late Quaternary Patagonian basalts (46–47°S): geochronometric and geochemical evidence for slab tearing due to active spreading ridge subduction. *J. Volcanol. Geotherm. Res.* 149, 346–370. doi: 10.1016/j.jvolgeores.2005.09.002

Hickey-Vargas, R. L., Frey, F. A., Gerlach, D. C., and López- Escobar, L. (1986). Multiple sources for basaltic arc rocks from the southern volcanic zone of the Andes (34°41'S): trace element and isotopic evidence for contributions from subducted oceanic crust, mantle and continental crust. *J. Geoph. Res.* 91, 5963–5983.

Hildreth, W., and Morbath, S. (1988). Crustal contributions to arc magmatism in the Andes of central Chile. *Contribut. Mineral. Petrol.* 98, 455–489.

Hofmann, A. W., and White, W. M. (1982). Mantle plumes from ancient oceanic crust. *Earth Planet. Sci. Lett.* 57, 421–436.

Höppner, N., Lucassen, F., Chiessi, C. M., Sawakuchi, A. O., and Kasemann, S. A. (2018). Holocene provenance shift of suspended particulate matter in the Amazon River basin. *Quat. Sci. Rev.* 190, 66–80.

Iannelli, S. B., Fennell, L. M., Litvak, V. D., Lucía, F. P., Alfonso, E., and Andrés, F. (2018). Geochemical and tectonic evolution of Late Cretaceous to early Paleocene magmatism along the Southern Central Andes (35-36°S). *J.South Am. Earth Sci.* 87, 139–156. doi: 10.1016/j.jsames.2017.12.008

Iannelli, S. B., Litvak, V. D., Fernández Paz, L., Folguera, A., Ramos, M. E., and Ramos, V. A. (2017). Evolution of Eocene to Oligocene arc-related volcanism in the North Patagonian Andes (39°-41°S), prior to the break-up of the Farallon plate. *Tectonophysics* 69, 70–87. doi: 10.1016/j.tecto.2016.12.024

Irvine, T. N., and Baragar, W. R. A. (1971). A guide to chemical classification of the common volcanic rocks. *Can. J. Earth Sci.* 8, 523–548.

Jacques, G., Hoernle, K., Gill, J., Wehrmann, H., Bindeman, I., and Lara, L. E. (2014). Geochemical variations in the central southern volcanic zone, chile (38–43 S): the role of fluids in generating arc magmas. *Chem. Geol.* 371, 27–45. doi: 10.1016/j.chemgeo.2014.01.015

Jacques, G., Hoernle, K., Gill, J. B., Hauff, F., Wehrmann, D., Garbe-Schönber, P., et al. (2013). Across-arc geochemical variations in the Southern Volcanic Zone, Chile (34.5–38°S): constraints on mantle wedge and source input compositions. *Geochim. Cosmochim.* 123, 218–243. doi: 10.1016/j.gca.2013.05.016

Jalowitzki, T., Gervasoni, F., Conceição, R. V., Orihashi, Y., Bertotto, G. W., Sumino, H., et al. (2017). Slab-derived components in the subcontinental lithospheric mantle beneath Chilean Patagonia: geochemistry and Sr–Nd–Pb isotopes of mantle xenoliths and host basalt. *Lithos* 292, 179–197.

Johnston, S. T., and Thorkelson, D. J. (1997). Cocos-Nazca slab window beneath central America. *Earth Planet. Sci. Lett.* 146, 465–474.

Jones, R. E., Kirstein, L. A., Kasemann, S. A., Litvak, V. D., Poma, S., Alonso, R. N., et al. (2016). The role of changing geodynamics in the progressive contamination of Late Cretaceous to Late Miocene arc magmas in the southern Central Andes. *Lithos* 262, 169–191. doi: 10.1016/j.lithos.2016.07.002

Jordan, T., Burns, W., Veiga, R., Pángaro, F., Copeland, P., Kelley, S., et al. (2001). Extension and basin formation in the Southern Andes caused by increased convergence rate: amid-Cenozoic trigger for the Andes. *Tectonics* 20, 308–324.

Kay, S. M., Burns, M., and Copeland, P. (2006). "Upper Cretaceous to Holocene magmatism and evidence for transient Miocene shallowing of the Andean subduction zone under the northern Neuquén Basin," in *Evolution of an Andean margin: A Tectonic And Magmatic View From The Andes To the Neuquén Basin (35–39° S)*, eds S. M. Kay and V. A. Ramos (London: The Geological Society),

Kay, S. M., Godoy, E., and Kurtz, A. (2005). Episodic arc migration, crustal thickening, subduction erosion, and magmatism in the south-central Andes. *Geol. Soc. Am. Bull.* 117, 67–88.

Kay, S. M., Ramos, V. A., and Marquez, M. (1993). Evidence in Cerro Pampa volcanic rocks for slab-melting prior to ridge-trench collision in southern South America. *J. Geol.* 101, 703–714.

Kleiman, L. E., and Japas, M. S. (2009). The Choiyoi volcanic province at 34 S–36 S (San Rafael, Mendoza, Argentina): implications for the Late Palaeozoic evolution of the southwestern margin of Gondwana. *Tectonophysics* 473, 283–299.

Ladino, M., Blanco, N., Matthews, S., and Tomlinson, A. J. (2000). "Cambios geoquímicos en el magmatismo del límite Cretácico- Terciario en la precordillera de Calama, II región de Antofagasta, norte de Chile" in IX Congreso Geológico Chileno. *Puerto Varas* 1, 630–634.

Le Maitre, R. W., Bateman, P., Dudek, A., Keller, J., Lameyre, J., and Le Bas, M. J. (1989). *A Classification of Igneous Rocks and Glossary of Terms: Recommendations of the International Union of Geological Sciences Subcommission on the Systematics of Igneous Rocks*. Oxford: Blackwell Scientific Publications.

Legarreta, L., and Uliana, M. A. (1991). Jurassic-Cretaceous marine oscillations and geometry of back-arc basin fill, central argentine andes, in sedimentation, tectonics and eustasy: sea-level changes at active margins. *IAS Spec. Publ.* 12, 429–450.

Litvak, V. D., Encinas, A., Oliveros, V., Bechis, F., Folguera, A., and Ramos, V. A. (2014). "El volcanismo mioceno inferior vinculado a las ingresiones marinas en los Andes Nordpatagónicos," in *Proceedings of the 19° Congreso Geológico Argentino*, Córdoba.

Litvak, V. D., Fernández Paz, L., Iannelli, S., Poma, S., and Folguera, A. (2019). "Cenozoic arc-related magmatism in the southern Central and North Patagonian Andes," in *Andean Tectonics*, eds B. Horton and A. Folguera (Amsterdam: Elsevier), 573–607. doi: 10.1016/B978-0-12-816009-1.00021-6

Litvak, V. D., Poma, S., and Kay, S. M. (2007). Paleogene and Neogene magmatism in the Valle del Cura region: new perspective on the evolution of the Pampean flat slab, San Juan province, Argentina. *J. South American Ear. Sci.* 24, 117–137. doi: 10.1016/j.jsames.2007.04.002

Litvak, V. D., Spagnuolo, M. G., Folguera, A., Poma, S., Jones, R. E., and Ramos, V. A. (2015). Late Cenozoic calc-alkaline volcanism over the Payenia shallow subduction zone, South-Central Andean back-arc (34° 30'–37° S), Argentina. *J. South Am. Earth Sci.* 64, 365–380.

Llambías, E. J., and Aragón, E. (2011). "Volcanismo Paleógeno", in *Proceedings of the Geología y Recursos Naturales de la Provincia del Neuquén in XVIII Congreso Geológico Argentino*, Neuquén.

Llambías, E. J., Bertotto, G. W., Risso, C., and Hernando, I. (2010). El volcanismo cuaternario en el retroarco de Payenia: una revisión. *Rev. Asoc. Geol. Argent.* 67, 278–300.

Llambías, E. J., Quenardelle, S. Y., and Montenegro, T. (2003). The Choiyoi group from central Argentina: a subalkaline transitional to alkaline association in the craton adjacent to the active margin of the Gondwana continent. *J. S. Am. Earth Sci.* 16, 243–257.

Llambías, E. J., and Rapela, C. W. (1989). Las vulcanitas de collipilli, neuquén, y su relación con otras unidades paleógenas de la cordillera. *Rev. Asoc. Geol. Argent.* 44, 224–236.

López-Escobar, L., Cembrano, J., and Moreno, H. (1995). Geochemistry and tectonics of the Chilean Southern andes basaltic quaternary volcanism (37-46°S). *Andean Geol.* 22, 219–234.

López-Escobar, L., Parada, M. A., Moreno, H., Frey, F. A., and Hickey-Vargas, R. L. (1992). A contribution to the petrogenesis of osorno and Calbuco volcanoes, southern Andes (41° 00'-41° 30'S): comparative study. *Andean Geol.* 19, 211–226.

López-Escobar, L., and Vergara, M. (1997). Eocene-Miocene longitudinal depression and quaternary volcanism in the Southern Andes, Chile (33-42.5 S): a geochemical comparison. *Andean Geol.* 24, 227–244.

Lucassen, F., Becchio, R., Harmon, R., Kasemann, S., Franz, G., Trumbull, R., et al. (2001). Composition and density model of the continental crust at an active continental margin in the Central Andes between 21° and 27°S. *Tectonophysics* 341, 195–223.

Lucassen, F., Escayola, M., Romer, R. L., Viramonte, J., Koch, K., and Franz, G. (2002). Isotopic composition of late mesozoic basic and ultrabasic rocks from the Andes (23–32°S): implications for the Andean mantle. *Cont. Mineral. Petrol.* 143, 336–349.

Lucassen, F., Trumbull, R., Franz, G., Creixell, C., Vásquez, P., Romer, R. L., et al. (2004). Distinguishing crustal recycling and juvenile additions at active continental margins: the paleozoic to recent compositional evolution of the Chilean Pacific margin (36–41 S). *J. South Am. Earth Sci.* 17, 103–119.

Maloney, K. T., Clarke, G. L., Klepeis, K. A., and Quevedo, L. (2013). The Late Jurassic to present evolution of the Andean margin: drivers and the geological record. *Tectonics* 32:67. doi: 10.1002/tect.20067

Mateo-Fernández Caso, M. P., Montero, D. G., Leal, P. R., and Ramos, V. A. (2011). Petrografía y geoquímica del magmatismo cretácico superior-eoceno en el área de pichaihue. *Provincia Neuquén. Rev. Asoc. Geol. Argent.* 68, 173–184.

Mella, M., Muñoz, J., Vergara, M., Klohn, E., Farmer, L., and Stern, C. R. (2005). Petrogenesis of the pleistocene tronador volcanic Group, Andean Southern Volcanic Zone. *Andean Geol.* 32, 131–154.

Melnick, D., Folguera, A., and Ramos, V. A. (2006). Structural control on arc volcanism: the Caviahue-Copahue complex (38°S). *J. S. Am. Earth Sci.* 22, 66–88.

Montecinos, P., Schärer, U., Vergara, M., and Aguirre, L. (2008). Lithospheric origin of Oligocene–Miocene magmatism in Central chile: U–Pb ages and Sr–Pb–Hf isotope composition of minerals. *J. Petrol.* 49, 555–580.

Montelli, R., Nolet, G., Dahlen, F. A., and Masters, G. (2006). A catalogue of deep mantle plumes: new results from finite-frequency tomography. *Geoch. Geophy. Geosyst.* 7:1248.

Mosolf, J. G. (2013). *Stratigraphy, Structure, And Geochronology Of The Abanico Formation In The Principal Cordillera, Central Chile: Evidence Of Protracted Volcanism And Implications For Andean Tectonics*. Ph. D. thesis, University of Santa Barbara, California, MA.

Mosolf, J. G., Gans, P. B., Wyss, A. R., Cottle, J. M., and Flynn, J. J. (2019). Late cretaceous to miocene volcanism, sedimentation, and upper-crustal faulting and folding in the principal cordillera, central Chile: field and geochronological evidence for protracted arc volcanism and transpressive deformation. *GSA Bulletin* 131, 252–273. doi: 10.1130/B31998.1

Mpodozis, C., Arriagada, C., Basso, M., Roperch, P., Cobbold, P., and Reich, M. (2005). Late mesozoic to paleogene stratigraphy of the salar de atacama basin, antofagasta, northern chile: implications for the tectonic evolution of the central andes. *Tectonophysics* 399, 125–154.

Müller, R. D., Seton, M., Zahirovic, S., Williams, S. E., Matthews, K. J., Wright, N. M., et al. (2016). Ocean basin evolution and global-scale plate reorganization events since Pangea breakup. *Annu. Rev. Earth Plant Sc.* 44, 107–138.

Munizaga, F., Hervé, F., Drake, R., Pankhurst, R. J., Brook, M., and Snelling, N. (1988). Geochronology of the Lake Region of south-central Chile (39–42 S): preliminary results. *J. S. Am. Earth Sci.* 1, 309–316.

Muñoz, J., Troncoso, R., Duhart, P., Crignola, P., Farmer, L., and Stern, C. R. (2000). The relation of the mid-Tertiary coastal magmatic belt in south-central Chile to the late oligocene increase in plate convergence rate. *Rev. Geol. Chile.* 27, 177–203.

Muñoz, M., Fuentes, F., Vergara, M., Aguirr, L., Olov Nyström, J., Féraud, G., et al. (2006). Abanico East Formation: petrology and geochemistry of volcanic rocks behind the Cenozoic arc front in the Andean Cordillera, central Chile (33° 50'S). *Rev. Geol. Chile.* 331, 109–140.

Muñoz, M., Tapia, F., Persico, M., Benoit, M., Charrier, R., Farías, M., et al. (2018). Extensional tectonics during Late Cretaceous evolution of the Southern central andes: evidence from the chilean main range at˜ 35° S. *Tectonophysics* 744, 93–117. doi: 10.1016/j.tecto.2018.06.009

Nullo, F. E., Stephens, G., Combina, A., Dimieri, L., Baldauf, P., Bouza, P., et al. (2005). *Hoja Geológica 3569-III Malargüe, Programa Nacional de Cartas Geológicas de la República Argentina a escala 1:250.000, Boletín 346*. Buenos Aires: SEGEMAR.

Obayashi, M., Yoshimitsu, J., Nolet, G., Fukao, Y., Shiobara, H., Sugioka, H., et al. (2013). Finite frequency whole mantle P wave tomography: improvement of subducted slab images. *Geophy. Res. Lett.* 40, 5652–5657.

Orts, D. L., Folguera, A., Giménez, M., Ruiz, F., Vera, E. A. R., and Klinger, F. L. (2015). Cenozoic building and deformational processes in the North patagonian andes. *J. Geodyn.* 86, 26–41.

Pankhurst, R. J., Rapela, C. W., Fanning, C. M., and Marquez, M. (2006). Gondwanide continental collision and the origin of Patagonia. *Earth Sci. Rev.* 76, 235–257.

Pankhurst, R. J., Weaver, S. D., Hervé, F., and Larrondo, P. (1999). Mesozoic–cenozoic evolution of the north patagonian batholith in aysén, Southern Chile. *Geol. Soc. Lond.* 156, 673–694.

Parada, M. A., Rivano, S., Sepúlveda, P., Hervé, M., Hervé, F., Puig, A., et al. (1988). Mesozoic and Cenozoic plutonic development in the andes of central Chile (30°30'-32°30S). *J. S. Am. Earth Sci.* 1, 249–260.

Pardo-Casas, F., and Molnar, P. (1987). Relative motion of the Nazca (Farallon) and South American plates since late Cretaceous time. *Tectonics* 6, 233–248.

Pearce, J. A. (1983). "Role of the sub-continental lithosphere in magma genesis at active continental margins," in *Continental Basalts and Mantle Xenoliths* eds C.J. Hawkesworth, and M.J. Norry (Nantwich, UK: Shiva Press), 230–249.

Piquer, J., Hollings, P., Rivera, O., Cooke, D. R., Baker, M., and Testa, F. (2017). Along-strike segmentation of the abanico basin, central chile: new chronological, geochemical and structural constraints. *Lithos* 268, 174–197.

Plimer, I. R., and Elliott, S. M. (1979). The use of Rb/Sr ratios as a guide to mineralization. *J. Geochem. Expl.* 12, 21–34.

Radic, J. P., Rojas, L., Carpinelli, A., and Zurita, E. (2002). "Evolución tectónica de la cuenca terciaria de Cura-Mallín, región cordillerana chileno argentina (36°30°-39°00°S)," in *Proceedings of the 15° Congreso Geológico Argentino*, Calafate.

Ramos, M. E., Folguera, A., Fennell, L., Giménez, M., Litvak, V. D., Dzierma, Y., et al. (2014). Tectonic evolution of the North patagonian andes from field and gravity data (39–40 S). *J. S. Am. Earth Sci.* 51, 59–75.

Ramos, V., and Kay, S. M. (1992). Southern Patagonian plateau basalts and deformation; back-arc testimony of ridge collisions. *Tectonophysics* 205, 261–282.

Ramos, V. A., and Folguera, A. (2005). "Tectonic evolution of the andes of neuquén: constraints derived from the magmatic arc and foreland deformation," in *The Neuquén Basin, Argentina: A case Study in Sequence Stratigraphy and Basin Dynamics*, Vol. 252, eds G. D. Veiga, A. Spalletti, J. A. Howell, and E. Schwarz (London: Geology Society), 15–35.

Rapela, C., Spalletti, L., Merodio, J., and And Aragón, E. (1984). "El vulcanismo paleoceno-eoceno de la provincia andino-patagónica," in *Geología y Recursos Naturales de la Provincia de Río Negro*, ed. V. Ramos (Buenos Aires: Geology Society), 189–214.

Rapela, C., Spalletti, L., Merodio, J., and Aragón, E. (1988). Temporal evolution and spatial variation of early Terciary volcanism in the Patagonian Andes (40°S-42°30'S). *J. S. Am. Earth Sci.* 1, 75–88.

Rapela, C. W., and Llambías, E. J. (1985). "La secuencia andesítica terciaria de Andacollo, Neuquén, Argentina," in *Actas 4° Congreso Geológico Chileno*, 458–488.

Rapela, C. W., Spalletti, L. A., and Merodio, C. J. (1983). Evolución magmática y geotectónica de la "Serie Andesítica" andina (paleoceno-eoceno) en la cordillera nordpatagónica. *Rev. Asoc. Geol. Argent.* 38, 469–484.

Rivera, O., and Mpodozis, C. (1991). "Volcanismo explosivo del Terciario inferior en la Precordillera de Copiapo Región de Atacama, Chile. Las calderas Lomas Bayas y Durazno" in *Proceedings of the VI Congreso Geológico Chileno*, Viña del Mar.

Rivera, O., and Mpodozis, C. (1994). *La Megacaldera Carrizalillo y sus Calderas Anidadas: Volcanismo Sinextensional Cretácico Superior-Terciario Inferior en la Precordillera de Copiapó" in VII°Congreso Geológico Chileno*. Concepción: University of Concepcion.

Rojas Vera, E. A., Folguera, A., Valcarce, G. Z., Giménez, M., Ruiz, F., Martínez, P., et al. (2010). Neogene to Quaternary extensional reactivation of a fold and thrust belt: the agrio belt in the southern central andes and its relation to the loncopué trough (38°–39°S). *Tectonophysics* 492, 279–294.

Rudnick, R. L., and Gao, S. (2003). Composition of the continental crust. *The crust* 3, 1–64.

Sagripanti, L., Vera, E. A. R., Gianni, G. M., Folguera, A., Harvey, J. E., Farías, M., et al. (2015). Neotectonic reactivation of the western section of the malargüe fold and thrust belt (tromen volcanic plateau, Southern Central Andes). *Geomorphology* 232, 164–181.

Salvioli, M., Lanfranchini, M. E., Recio, C., and de Barrio, R. E. (2017). El magmatismo cretácico-terciario y su relación con sistemas hidrotermales polimetálicos en la región de colipilli-naunauco, provincia del Neuquén. *Rev. Asoc. Geol. Arg.* 75, 46–63.

Santosh, M., and Kusky, T. (2010). Origin of paired high pressure–ultrahigh-temperature orogens: a ridge subduction and slab window model. *Terra Nova.* 22, 35–42.

Sato, A. M., Llambías, E. J., Basei, M. A., and Castro, C. E. (2015). Three stages in the Late Paleozoic to Triassic magmatism of southwestern Gondwana, and the relationships with the volcanogenic events in coeval basins. *J. S. Am. Earth Sci.* 63, 48–69.

Scasso, J. A. (2012). *Geología del Sector Oriental Del Lago Huechulafquen Y Nacientes Del Río Chimehuín, Comarca Junín De Los Andes, Provincia del Neuquén*. Master thesis, University of Buenos Aires, Buenos Aires.

Serra-Varela, S., González, P. D., Giacosa, R. E., Heredia, N., Pedreira Rodríguez, D., Martín González, F., et al. (2019). Evolution of the Palaeozoic basement of the North Patagonian Andes in the San Martín de los Andes area (Neuquén, Argentina): petrology, age and correlations. *Andean Geol.* 46, 102–130.

Seton, M., Müller, R. D., Zahirovic, S., Gaina, C., Torsvik, T., Shepard, G., et al. (2012). Global continental and ocean basin reconstructions since 200 Ma. *Earth Sci. Rev.* 113, 212–270.

Shephard, G. E., Matthews, K. J., Hosseini, K., and Domeier, M. (2017). On the consistency of seismically imaged lower mantle slabs. *Sci. Rep.* 7:10976. doi: 10.1038/s41598-017-11039-w

Silvestro, J., and Atencio, M. (2009). La cuenca cenozoica del río grande y palauco: edad, evolución y control estructural, faja plegada de malargüe. *Rev. Asoc. Geol. Arg.* 65, 154–169.

Søager, N., Holm, P. M., and Llambías, E. J. (2013). Payenia volcanic province, southern mendoza, Argentina: OIB mantle upwelling in a backarc environment. *Chem. Geol.* 349, 36–53.

Somoza, R., and Ghidella, M. E. (2005). Convergencia en el margen occidental de América del Sur durante el Cenozoico: subducción de las placas de Nazca, Farallón y Aluk. *Rev. Asoc. Geol. Argent.* 60, 797–809.

Somoza, R., and Ghidella, M. E. (2012). Late Cretaceous to recent plate motions in western South America revisited. *Earth Planet. Sci. Lett.* 33, 152–163. doi: 10.1016/j.epsl.2012.03.003

Somoza, R., Tomlinson, A. J., Caffe, P. J., and Vilas, J. F. (2012). Paleomagnetic evidence of earliest Paleocene deformation in Calama (22° S), northern Chile: andean-type or ridge-collision tectonics? *J. S. Am. Earth Sci.* 37, 208–213.

Somoza, R., and Zaffarana, C. B. (2008). Mid-Cretaceous polar standstill of South America, motion of the Atlantic hotspots and the birth of the Andean cordillera. *Earth Planet. Sci. Lett.* 271, 267–277.

Spagnuolo, M. G., Folguera, A., Litvak, V. D., Rojas Vera, E. A., and Ramos, V. A. (2012). Late Cretaceous arc rocks in the Andean retroarc region at 36.5°S: evidence supporting a Late Cretaceous slab shallowing. *J. S. Am. Earth Sci.* 38, 44–56.

Steinberger, B., Trond, H. T., and Thorsten, W. B. (2012). Subduction to the lower mantle-a comparison between geodynamic and tomographic models. *Solid Earth* 3, 415–432.

Suárez, M., and Emparán, C. (1995). The stratigraphy, geochronology and paleophysiography of a Miocene fresh water interarc basin. *S. Chile. J. S. Am. Earth Sci.* 8, 17–31.

Sun, S. S., and McDonough, W. F. (1989). "Chemical and isotopic systematics of oceanic basalts: implications for mantle composition and processes," in *Magmatism in Ocean Basins*, eds A. D. Saunders and M. J. Norry (London: Geological Society), 313–345.

Tapia, F. (2015). *Evolución Tectónica Y Configuración Actual De Los Andes Centrales Del Sur (34° 45'-35° 30'S)*. Ph. D. thesis, Universidad de Chile, Santiago.

Tapia, F., Farías, M., Naipauer, M., and Puratich, J. (2015). Late Cenozoic contractional evolution of the current arc-volcanic region along the southern Central Andes (35° 20' S). *J. Geod.* 88, 36–51.

Tesoniero, A., Auer, L., Boschi, L., and Cammarano, F. (2015). Hydration of marginal basins and compositional variations within the continental lithospheric mantle inferred from a new global model of shear and compressional velocity. *J. Geophy. Res. Solid Earth* 120, 7789–7813.

Thorkelson, D. J. (1996). Subduction of diverging plates and the principles of slab window formation. *Tectonophysics* 255, 47–63.

Turienzo, M., Dimieri, L., Frisicale, C., Araujo, V., and Sánchez, N. (2012). Cenozoic structural evolution of the Argentinean Andes at 34 40'S: a close relationship between thick and thin-skinned deformation. *Andean Geol.* 39, 317–357.

Turienzo, M. M. (2010). Structural style of the Malargüe fold-and-thrust belt at the Diamante River area (34° 30'–34° 50' S) and its linkage with the cordillera frontal, andes of central Argentina. *J. S. Am. Earth Sci.* 29, 537–556.

Turner, J. C. M. (1973). Descripción geológica de la Hoja 37 a-b, Junín de los Andes, provincia del Neuquén. *Serv. Nacional Minero Geol. Boletín* 138, 1–86.

Utgé, S., Folguera, A., Litvak, V., and Ramos, V. A. (2009). Geología del sector norte de la cuenca de Cura Mallín en las lagunas de Epulaufquen. *Neuquén. Rev. Asoc. Geol. Argent.* 64, 231–248.

van der Meer, D. G., Spakman, W., van Hinsbergen, D. J. J., Amaru, M. L., and Torsvik, T. H. (2010). Towards absolute plate motions constrained by lower-mantle slab remnants. *Nat. Geosci.* 3, 36–40.

van der Meer, D. G., Torsvik, T. H., Spakman, W., van Hinsbergen, D. J. J., and Amaru, M. L. (2012). Intra-Panthalassa Ocean subduction zones revealed by fossil arcs and mantle structure. *Nat. Geosci.* 5, 215–219.

van der Meer, D. G., van Hinsbergen, D. J., and Spakman, W. (2018). Atlas of the underworld: slab remnants in the mantle, their sinking history, and a new outlook on lower mantle viscosity. *Tectonophysics* 723, 309–448.

Varela, R., Basei, M. A. S., Cingolani, C. A., and Passarelli, C. R. (2005). El basamento cristalino de los Andes norpatagónicos en Argentina: geocronología e interpretación tectónica. *Rev. Geol. Chile.* 32, 167–187.

Varela, R., Teixeira, W., Cingolani, C., and Dalla Salda, L. (1994). "Edad Rubidio-Estroncio de granitoides de Aluminé-rahue, cordillera norpatagónica, Neuquén, Argentina," in *Proceedings of the VII°Congreso Geológico Chileno*, Concepción.

Wehrmann, H., Hoernle, K., Garbe-Schönberg, D., Jacques, G., Mahlke, J., and Schumann, K. (2014). Insights from trace element geochemistry as to the roles of subduction zone geometry and subduction input on the chemistry of arc magmas. *Int. J. Ear. Sci.* 103, 1929–1944. doi: 10.1007/s00531-013-0917-1

Windley, B. F., and Xiao, W. (2018). Ridge subduction and slab windows in the Central Asian orogenic belt: tectonic implications for the evolution of an accretionary orogen. *Gondwana Res.* 61, 73–87.

Wright, N. M., Seton, M., Williams, S. E., and Müeller, R. D. (2016). The late cretaceous to recent tectonic history of the pacific ocean basin. *Earth Sci. Rev.* 154, 138–173.

Xia, L., and Li, X. (2019). Basalt geochemistry as a diagnostic indicator of tectonic setting. *Gondwana Res.* 65, 43–67.

Zamora Valcarce, G., Zapata, T., del Pinto, A., and Ansa, A. (2006). "Structural evolution and magmatic characteristics of the Agrio fold-and-thrust belt," in *Evolution of an Andean Margin: A Tectonic And Magmatic View From The Andes To The Neuquén Basin (35–39°S)*, Vol. 407, eds S. M. Kay and V. A. Ramos (London: Geological Society), 125–146.

Zartman, R. E., and Doe, B. R. (1981). Plumbotectonics—the model. *Tectonophysics* 75, 135–162.

Zindler, A., and Hart, S. (1986). Chemical geodynamics. *Ann. Rev. Earth Planet. Sci.* 14, 493–571.

Conflict of Interest: The authors declare that the research was conducted in the absence of any commercial or financial relationships that could be construed as a potential conflict of interest.